Emissions reduction by using e-components in 48 V mild hybrid trucks under dual-mode dual-fuel combustion

Antonio García[a], Javier Monsalve-Serrano[*, a], Santiago Martinez-Boggio[a], Patrick Gaillard[b]

[a]CMT - Motores Térmicos, Universitat Politècnica de València, Camino de Vera s/n, 46022 Valencia, Spain
[b]Aramco Fuel Research Center, Aramco Overseas Company B.V. Paris, France

Corresponding author (*):
Dr. Javier Monsalve-Serrano (jamonse1@mot.urpv.es)
Phone: +34 963876559
Fax: +34 963876559

Abstract

The European community foresees a 15% CO_2 tailpipe emissions restriction in 2025 and 30% in 2030 for the trucks. While battery electric vehicles would help to reach these levels, their low ranges make them unfeasible for the good transport sector. By this reason, hybrid vehicles are considered the bridge between the current technology and the battery electric vehicles. The 48 V mild hybrid technology is an effective solution due to its low cost and changes needed with respect to the current technology. It also allows the use of electrical components that help to improve the brake thermal efficiency, reduce the emissions and recover energy. This works explores the potential of an electric turbo compound (e-TC) and an electric exhaust gas recirculation pump (e-EGR pump) in a mild hybrid truck platform working under dual-mode dual-fuel (DMDF) combustion with diesel and gasoline. The e-components are simulated by means of 0D-Engine modeling. Finally, a general overview of the potential in real applications is done by means of a vehicle model considering different driving cycles and truck payloads for two truck platforms (18-ton and 25-ton maximum payload). The results show that to achieve the large EGR rates required by the DMDF combustion and meet the air requirements, it necessary the use of both e-components together. The evaluation at vehicle conditions allows to conclude that the mild hybrid platform allows to reduce the CO_2 emissions around 6% in homologation conditions and 10% in urban cycles. Moreover, it was found that the use of e-components only improves the vehicle efficiency in the cases with low truck payloads.

Keywords

e-components, Mild Hybrid, dual-fuel, Emissions regulations, Driving cycles

1. Introduction

Nowadays, fossil fuels are the best on-board energy sources in vehicles in terms of energy density and refueling time [1]. However, the high increase of global temperature together with the increase of transported goods in recent years has forced regulatory authorities around the world to establish strict regulations on the CO_2 emissions [2]. These scenarios are challenging for the vehicle manufacturers but create an ideal space for the development of new technologies and concepts. Heavy-duty road transportation is responsible for about 25% of the CO_2 emissions from road transport in the EU and for some 5% of total EU emissions [3]. Despite the improvements achieved in fuel consumption during the recent years, the global CO_2 emissions are still rising, mainly due to an increase in the road freight traffic [4]. Therefore, the reduction of the local and global emissions of this type of vehicles is crucial [5]. One option is the use of pure electric powertrains, but the large-scale application faces the barriers of the high cost of electrical energy storage in batteries and range limitations [6]. These barriers can be reduced by the use of hybrid powertrains [7]. Hybrid electric vehicles (HEVs) can operate more efficiently than the internal combustion engine (ICE) set points. In addition, options as downsized or component simplification while fulfilling the same maximum power requirements are possible [8]. Other benefits of the HEVs come from the energy recuperation during braking by means of an electric machine as well as the possibility to optimize the energy management between several power sources [9]. Lastly, the introduction of high energy storage sources as the Lion-Ion batteries allows the development of new technologies as electrified components (e-components) [10]. Some examples that appeared in the last years are the electric turbo compound (e-TC) [11] and electric exhaust gas recirculation pump (e-EGR pump) [12] or electric heaters in the aftertreatment system (e-ATS) [13], among others. These elements contribute to increase the potential of the HEV to reduce the fuel consumption and tailpipe emissions as compared to the ICE-propelled vehicles.

In a conventional vehicle, 30%–40% of energy is lost in the exhaust gas [14]. Various waste-heat recovery systems (WHRS) are currently used by different vehicle manufacturers or mentioned in the literature to increase the total ICE efficiency. Examples are an organic Rankine cycle [9], thermoelectric generation [15] and turbocompounding [16], among other devices. The last application mentioned takes advantage of the exhaust gas energy in a turbine to boost the air pressure entering to the engine by means of a compressor. This is the most common solution used in commercial vehicles due to the large benefits and simple operation. Different solutions exist to regulate the operation of this system. The simplest, but less efficient, way is the use a waste gate that bypasses the excess of energy in the turbine. A better, but more complex, option is the variable-geometry turbine (VGT), which modifies the turbine effective diameter by modifying the blades opening to allow the turbocharger working in a wide range of engine speeds [17]. However, this cases also introduces energy losses. Another problem of the turbochargers is the poor transient response during the vehicle acceleration, which is called turbo-lag [10]. Therefore, in the last years it was proposed to couple an electric machine (EM) to the turbocompounding shaft. The EM can be operated as a generator to recover the wasted part of the exhaust energy as electric power [18]. In addition, it improves the turbocharger reaction by generating boost pressure when the throttle shifts rapidly or can achieve high-pressure boost with little

exhaust energy. Therefore, hybrid powertrains provide an excellent environment for the application of electrified turbochargers. Zi et al [16] studied a new electric turbo-compounding layout called electric-booster and turbo-generator system (EBTG) in a 1.5 liter spark ignition engine. The turbo and compressor operate independently with two electric motors. The maximum reduction of fuel consumption was 2.6% at high engine speed and load. The exergy analysis showed that the EBTG system can reduce the irreversibility in the turbine and recovery more exergy from the exhaust gas. The step time response of the boost pressure in the EBTG engine decreased to about half. However, at low and medium loads, a 4% increase of the fuel consumption was found. Similar results were given by Pasini et al. [10] using a 0.9 liter spark ignition engine with an e-TC layout (turbine and compressor in the same shaft with an EM). However, the use of this technology in compression ignition (CI) engines nor under low temperature combustion modes has not been reported yet in literature.

Exhaust gas recirculation is one of the most effective methods to reduce the combustion chamber temperatures and thereby to reduce the NOx formation [19]. In the presence of a turbocharger, there are two ways to obtain the EGR. If the gas flow is taking at the turbine inlet and sent to the compressor outlet, then it is called high pressure EGR (HP-EGR). The main advantages of this solution are the engine packaging, the fast effect on the combustion process and emissions, and the avoidance of the gas passing through the compressor. The major drawback of the HP-EGR system are the high EGR temperature and the energy reduction at the turbine inlet [20]. On the contrary, the low pressure EGR (LP-EGR) is took at the turbine outlet and sent to the compressor inlet [21]. The advantage of this method is that it does not reduce the energy available at the turbine inlet and the EGR temperature is colder than HP-EGR, with higher benefits in terms of NOx emissions [22]. However, the longer route to the engine reduces the response and the gas needs to be cleaned of particle matter and water to avoid damaging the compressor. Therefore, the HP-EGR is more used in commercial applications. Moreover, the low temperature combustion (LTC) modes use much higher EGR rates than conventional diesel combustion (CDC) to strongly reduce NOx emissions [23]. Through the different LTC concepts, the reactivity controlled compression ignition (RCCI) combustion can be highlighted as one of the most promising concepts due to the balance between fuel consumption, emissions and operating range [24]. This concept is based on using two fuels with different reactivity, allowing to generate a stratification of temperature and mixture reactivity inside the combustion chamber. This provides a greater control degree on the combustion development compared to other concepts as the HCCI, which relies only in thermal stratification [25]. To reduce the emissions, high amounts of low reactivity fuel (e.g. gasoline, ethanol, methanol, etc.) need to be injected in the intake ports and high exhaust gas recirculation rates are needed in the combustion chamber [26]. In spite of that, large pressure gradients are found with RCCI at high loads, so that the DMDF concept has been proposed to cover the complete engine map. Despite being in a development phase, dual mode dual-fuel (DMDF) is one of the most promising concepts due to the ultra-low NOx and particle matter emissions together with high brake efficiency [27]–[29]. To achieve the required EGR rates, a solution proposed by Garcia et al. [30] is to use both systems, HP-EGR and LP-EGR. Another option recently proposed by Eaton [12] is the use of a e-EGR pump driven by a 48-volt electric motor, making it completely independent from engine speed and significantly more controllable than pump-less EGR systems. This technology enables high EGR flows

in operating regions where it wasn't possible to drive flow before and provides more accurate EGR flow rate control for better combustion and emissions management. This setup allows the turbocharger to be optimized for the maximum boosting efficiency without being compromised by the need to drive the EGR. Additionally, because the pump can maintain any desired EGR flow rate, it can play an important role for the development of emerging advanced combustion modes as RCCI [31]. Due to the recent appearance of this technology, no works can be found in the literature up to the knowledge of the authors.

The use of e-components is an attractive technology for an efficient propulsion, helping the new combustion concepts to achieve the desired robustness to be applied in commercial applications. The lack of research in the area of electrified components for engines operating under low temperature combustion modes motivates the publication of this research. Thus, the aim of this paper is to show the potential of e-TC and e-EGR pump in a multi-cylinder engine working under DMDF combustion intended for truck applications. In particular, the main goal is to evaluate the possibility of removing the LP-EGR line thanks to the use of the e-components. Engine and vehicle numerical modeling are built-up starting from experimental tests of the DMDF concept without e-components. Then, three powertrain variations are simulated: only e-TC, only e-EGR pump and both e-components. The best solution is selected after a study in the six most representative engine calibration points. All the results are compared to the case that does not use any e-component, in two versions: HP+LP EGR line and only HP EGR line. Later, the optimum case is studied in 36 operative points trying to optimize fuel economy. The electric losses are considered in the final calculation. Lastly, four driving cycles at several payloads are simulated for two truck platforms.

2. Methodology

The evaluation of the potential a 48V mild hybrid DMDF medium-duty truck in transient conditions is performed with a 0D-vehicle model. The non-hybrid OEM diesel truck platform is used for comparison. The ICE is modeled with a map-based approach to predict the vehicle fuel consumption and engine-out emissions with and without e-components. The engine maps for the two cases (Diesel and DMDF) without e-components were obtained in an engine test bed. Later, the engine maps for the DMDF including the use of e-components were obtained with a 0D-ICE detailed model previously calibrated with experimental data. To do this, the e-TC and e-EGR pump models were added to the original 0D-ICE platform and optimized to obtain the minimum energy consumption. In this sense, both liquid fuel and electric energy consumption are considered in the energy balance. The optimum configuration is analyzed in four driving cycles representative of the homologation and real driving conditions. The engine, e-components and vehicle models are detailed in the next sections.

2.1. Engine model

The OEM engine is an 8 L direct injection CI diesel engine with a VGT and high pressure EGR that equips different ATS to fulfill the EUVI emissions regulation (Urea-selective catalytic reaction for NOx, diesel particulate filter for particle matter and soot, and diesel oxidation catalyst for HC and CO).

The use of the DMDF combustion is intended to achieve high fuel economy while fulfilling the EUVI emissions legislation only requiring a diesel oxidation catalyst (DOC) as ATS. To do so, the DMDF concept uses pure RCCI at low and medium engine loads and a dual-fuel diffusive combustion at full load, where the RCCI mode cannot be applied due to excessive combustion peak pressures. Diesel is used as high reactivity fuel (HRF) injected directly in the combustion chamber (OEM injection system) and gasoline is used as LRF to be injected through the PFI system. To achieve the required EGR rates (double or triple than with CDC) without impairing the turbocompounding performance, a low pressure EGR line was used in previous works [32]. In this work it is proposed an alternative method by using an e-EGR pump installed in the original HP-EGR line. The use of the e-EGR pump together with the LP EGR is not considered because implies large EGR rates flowing through the compressor, which drops the efficiency and implies the use of a dedicated DPF for the compressor safety. Other possibility would be to connect the e-EGR pump between the turbine outlet and the compressor outlet. However, the e-EGR pump considered is a positive displacement pump that cannot achieve high pressure increase.

Moreover, the addition of an e-TC is considered to maximize the potential of the system. The main characteristics of the different engine versions analyzed are detailed in Table 1.

Table 1 – Main engine specifications for the different engine versions equipped in the truck.

Parameter	CDC ICE	DMDF ICE	DMDF ICE with e-components
Type [-]	4 stoke, 4 valves		
Nº Cylinders [-]	6		
Displaced Volume [cm^3]	7700		
Stroke [mm]	135		
Bore [mm]	110		
Injection type & Fuel [-]	DI diesel	DI diesel - PFI gasoline	
Compression ratio [-]	17.5	12.8	
High pressure EGR [-]	Yes	Yes	e-EGR pump
Low pressure EGR [-]	No	Yes	No
Turbo Configuration [-]	VGT		e-TC+VGT
Rated Power [hp]	350 @2200 rpm		
Rated Torque [Nm]	1400 @1200 to 1600 rpm		

An experimental test campaign was performed in order to obtain the fuel consumption and emissions in 36 operative conditions in a range of 950-2200 rpm and 0-100% engine load for the two first ICE versions of Table 1. The main results of the calibration maps are illustrated in Figure 1, Figure 2 and Figure 3. As the aim of the work is to see the benefits of the DMDF concept against the OEM CDC, the difference values between both calibrations are presented in the maps. Figure 2a shows that the absolute differences in EGR rate are between 10% and 30%, higher for DMDF than CDC. Figure 2b shows the gasoline fraction (GF) as the percentage of gasoline over the total mass injected per cylinder, which shows peak values of 90%. The lower GF are found below 50 hp, where greater diesel amount is needed due to the low reactive in-cylinder conditions. At medium load, where pure RCCI strategy is applied, the GF achieves values up to 90%. In the upper part of the map (above 210 hp), the diffusive dual-fuel mode is implemented with lower EGR rates and GF ratios than with the RCCI strategy. As shown

in Figure 2, this strategy allows to achieve very low engine-out emissions, with a decrease of NOx in all the map and lower soot in almost all the conditions (with the exception of some high load points). In particular, the EU VI legislation can be achieved for both pollutants (NOx and soot) up to 210 hp without the need for dedicated ATS. At higher loads, due to the diffusive part of the combustion process, the soot increases far above the EU VI (10 mg/kWh). Also, as the EGR rate is reduced to avoid excessive soot, the NOx also increases above EU VI (0.4 g/kWh). Despite this increment, it is interesting to note that DMDF can achieve the same maximum power than CDC with a strong reduction of NOx and soot emissions and similar fuel economy. Figure 3 shows the difference in terms of brake specific fuel consumption (BSFC) between the DMDF and CDC. From the figure, it is seen that the BSFC can be reduced up to 10 g/kWh in the pure RCCI zone, while maximum penalties around 15 g/kWh are found at low engine speed and loads, and low engine speed and high loads. This is explained by the appearance of pressure gradient limitations that limits the possibility to well phase the combustion in the cycle together with the five lower compression ratio points compared to CDC. More insights on the boost pressure, injection timings and combustion parameters can be found in the Appendix A and in a previous work of the research group [30].
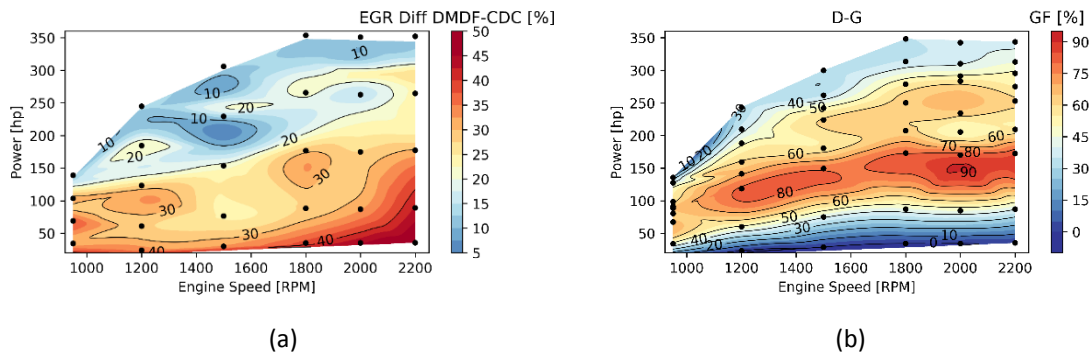

(a)   (b)

Figure 1- EGR rate maps difference between DMDF HP+LP EGR and CDC (a) and GF in DMDF HP+LP EGR (b).

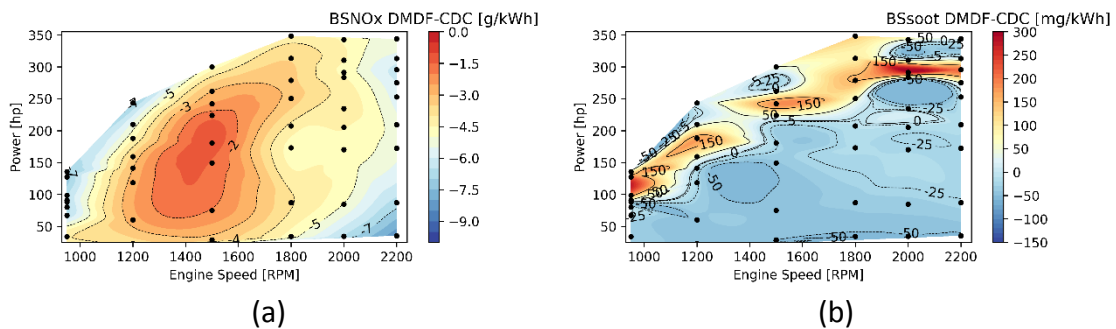(a)   (b)

Figure 2- BSNOx (a) and BSsoot (b) maps difference between DMDF HP+LP EGR and CDC.
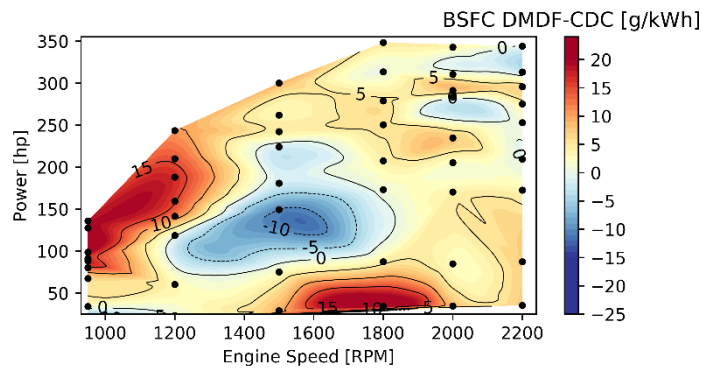
Figure 3- Brake specific fuel consumption map difference between DMDF HP+LP EGR and CDC.

After the experimental campaign, a detailed 0D-ICE model is built including all the components (turbocompounding, EGR lines, injection system and heat exchanger, among others). The modelling work is performed in GT-Suite v2020 (Gamma Technologies) [33]. Figure 4 shows the GT-Power model scheme for the DMDF ICE tested in the experimental engine test bench. The pipes and heat exchanger are designed following the real dimensions. The in-cylinder pressure traces and average pressure-temperature measurements in the intake and exhaust lines during the experimental test campaign are used to calibrate the heat exchanged and pressure losses model in each component. For the calibration of the air management system, 10 representative operating points are used. The other 26 points are used for validation. The combustion process is modeled by imposing the heat release rates obtained after post-processing the in-cylinder pressure of the experimental campaign. The turbine and compressor are modeled by means of the turbomachines maps in terms of speed, mass flow rate, pressure ratio and efficiency. For the turbine, it is necessary to add a map for each blade position due to the variable geometry layout. For this work, six maps with positions referring to 0%, 25%, 50%, 75% and 100% of the VGT opening are used, which were obtained in a flux bench for turbocompounding characterization. The ATS system pressure drop is considered in the experiments by means of a back-pressure valve and reproduced in the numerical model by means of an exhaust ambient condition block. This calibration is fundamental for the prediction of the ICE behavior when the e-components are added to the model.
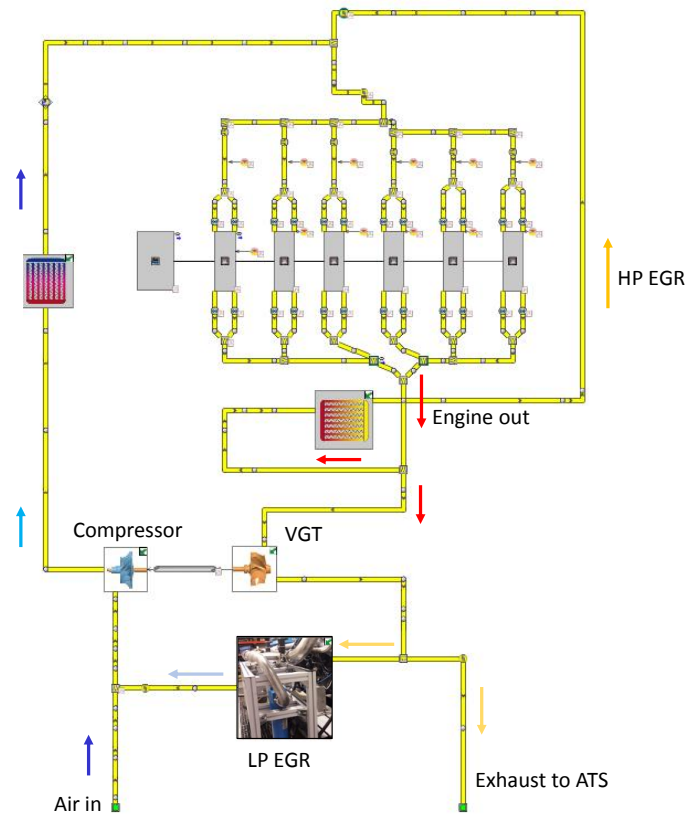
Figure 4 – 0D-engine model for the DMDF ICE configuration with LP and HP EGR lines.

Figure 5 Figure shows the in-cylinder pressure versus volume (p-v diagram) trace for the experimental and simulated cases at 950 rpm and 25% engine load. It is possible to see a good agreement between the experimental and simulated cases with an accurate match in the pumping phase as well as in the compression and expansion strokes. Appendix A contains more information about other validation points at different engine speeds and loads.
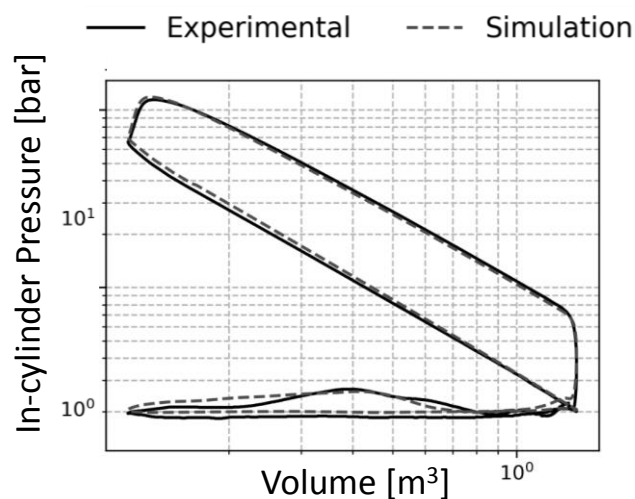

Figure 5 – Pressure-volume diagram including the experimental and simulation traces for 950 rpm and 25% of engine load (brake power of 35 hp) for the DMDF LP+HP EGR configuration.

Figure 6 shows the results for all the operative conditions in terms of indicated and brake mean effective pressure (IMEP and BMEP). In addition, inlet conditions in the turbine are shown in Figure 7. The R-squared is above 0.90 for all the parameters, confirming good agreement between experimental and numerical data.
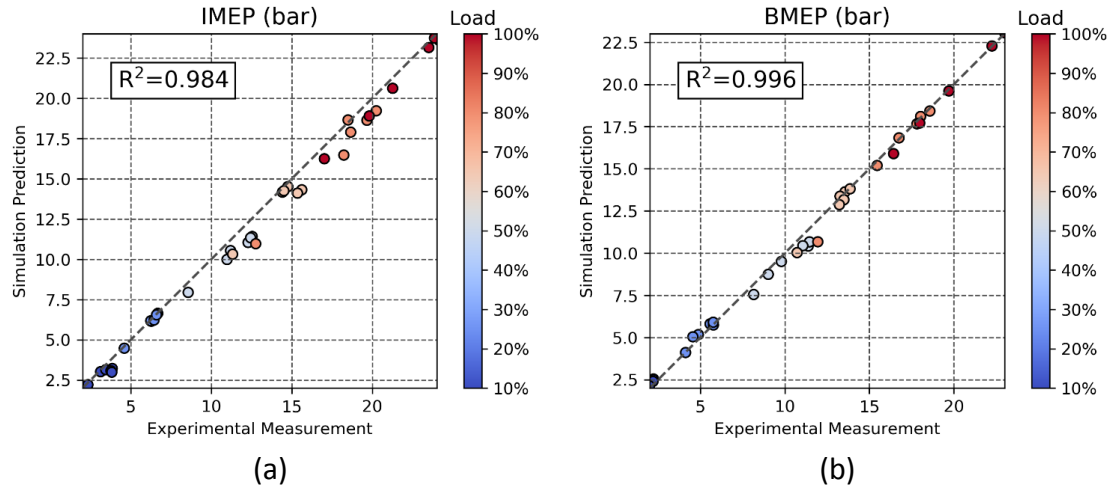

(a)   (b)

Figure 6 – Experimental versus simulation results of the 0D-engine model for DMDF LP+HP EGR configuration in terms of IMEP (a) and BMEP (b).
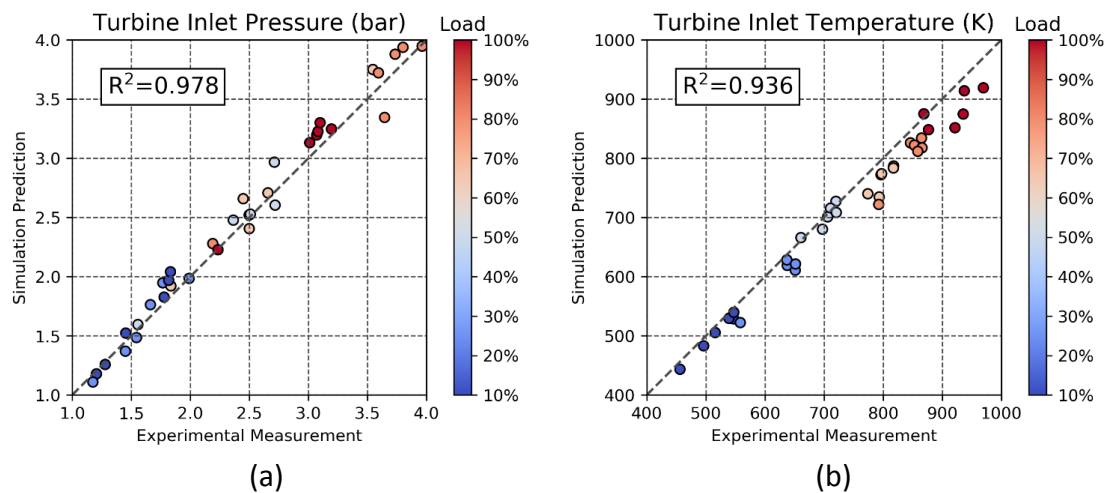

(a)   (b)

Figure 7 - Experimental versus simulation results of the 0D-engine model for DMDF LP+HP EGR configuration in terms of turbine inlet pressure (a) and turbine inlet temperature (b).

After the engine model validation, it is possible to add the e-components in the model. The aim of these new components is to allow the same in-cylinder conditions of the DMDF ICE without using the LP-EGR line. Therefore, it is necessary to achieve the same intake pressure and temperature as well as the composition of the gasses. This allows to maintain the same heat release rates and emissions prediction than in the case without e-components.

2.2. e-Components models

The e-EGR pump, located in the HP-EGR line, is in charge of delivering all the necessary EGR to the cylinder. In the DMDF ICE it was done originally by the addition of HP-EGR and LP-EGR. To achieve the EGR target with e-components, a proportional–

integral–derivative (PID) controller is added in the control system with a signal of the current and the target EGR of the DMDF calibration. The PID signal actuates on the e-EGR pump speed. If more EGR rate is necessary, the pump will accelerate consuming energy from the battery. In the case of excess of EGR rate, the e-EGR pump can recovery energy by braking the shaft (reducing the rotational pump speed). As the e-EGR pump operation is independent of the engine speed, it allows an extra degree of freedom to deliver or recover electric energy.

The electric turbocompounding is achieved by adding an electric motor in the shaft of the original VGT [34]. The main objective of this component is to achieve the same boost pressure obtained in the DMDF calibration. Similar to the EGR, to achieve the desired boost pressure, a PID is added in the control system with a signal of the current mean boost pressure and the target of the DMDF calibration. The signal acts on the torque of the electric machine to slow it down if the boost pressure is above the target or deliver power if it is below the target. The blades position is fixed in each simulation case. Therefore, a parametric study for this parameter is done.

Both components are modeled with prototypes available in the market and fed with a 48V electric system. In the following section, the complete vehicle model, the 48V battery pack and the belt alternator starter (BAS) are explained.

As was mentioned, the model is valid under the assumption that the conditions at intake valve closing must be the same than in the original DMDF engine calibration without e-components. This means equal injection mass, gasoline fraction, EGR composition and temperature among others. This allows to assume that equal combustion process occurs in both models. Therefore, the heat release rate and emissions are maintained. Also, maximum safe turbine inlet pressure (<3.8 bar) and temperature (<1270 K) and compressor inlet temperature (<450 K) need to be met. To guarantee this, the cases that do not meet this condition are eliminated during the data post-processing. Figure 8 shows a scheme of the GT-Power 0D engine model with the e-components.
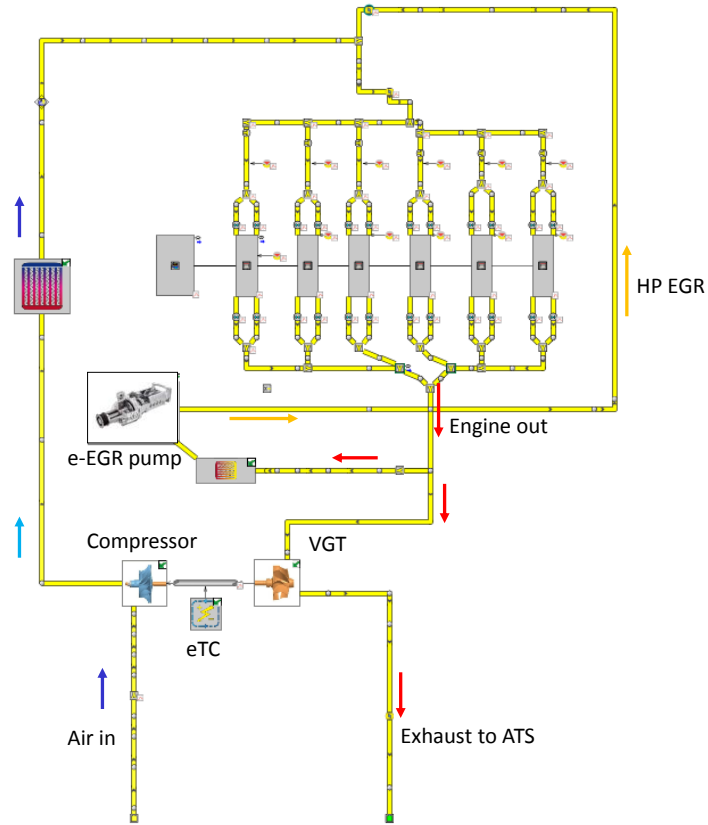
Figure 8 - 0D-engine model for the DMDF with e-components (e-EGR pump in the HP EGR line and the e-TC).

The e-EGR pump is a positive displacement pump, which produces flow just slightly above the intake pressure. The model is based on a prototype recently lunch by Eaton [12]. As mentioned, the e-EGR pump is driven by a 48V electric motor that makes the rotational speed completely independent from the engine speed.

$$Q_{real} = w.D.\eta_{vol} \tag{1}$$

$$W = \frac{\Delta P.Q_{real}.\eta_{electric}}{\eta_{isentropic}}, \Delta P > 0 \quad or \quad W = \frac{\Delta P.Q_{real}.\eta_{isentropic}}{\eta_{electric}}, \Delta P < 0 \tag{2}$$

with Q_{real} the volumetric flow through the pump, w the rotational speed of the pump, $D = 400 \, cm^3$ the displacement of the pump and $\eta_{vol} = 0.90$ the volumetric efficiency. W is the power of the pump with two conditions depending on the pressure difference between inlet and outlet (ΔP). The isentropic efficiency $\eta_{isentropic} = 0.40$ is also needed for the power calculation. The electric efficiency in the pump ($\eta_{electric}$) is estimated as 96%.

The e-TC is modeled as an electric machine coupled to the turbocompounding shaft as shown in Figure 8. This allows to deliver or recover power depending on the engine inlet and outlet conditions and the calibration targets. Due to the high rotational speed of the turbocompounding, a gear reduction of 3 is included in the electric machine design. For the control of this device, two parameters are considered. One signal

corresponds to the blade position and other to the electrical power delivery. The first signal will be calibrated in this work by means of a design of experiments (DoE). The second signal is calculated by means of a PID with the current intake manifold pressure and the target intake pressure for the DMDF ICE configuration. The maximum brake power of the e-TC electric machine is set at 15 kW and maximum allowed speed of 60000 rpm.

Therefore, the main parameter to be found is the optimal blade position to achieve the same condition of the DMDF ICE configuration with maximum equivalent brake specific fuel consumption of the engine. It is important to note that this last parameter is measured in terms of fuel mass consumption ($\dot{m}_{fuel}$), brake power ($Power_{ICE\ brake}$) and net electrical power ($Power_{e-components}$), as shown in Equation (3):

$$BSFC_{eq} = \frac{\dot{m}_{fuel}}{Power_{tot}} = \frac{\dot{m}_{fuel}}{Power_{ICE\ brake} + Power_{e-components}} \quad (3)$$

To understand the effect of each e-component a preliminary evaluation in 6 operative points is done with only e-TC, only e-EGR pump and e-TC + e-EGR pump. A sweep of the VGT position is done with 10 different cases for each operative condition (180 total cases). After the selection of the optimum setup of e-components, the optimization in the 36 operative conditions is performed by means of a design of experiments (DoE) with 360 cases of study, as shown in Figure 9. After the selection of the optimum setup of the e-components, the optimization in the 36 operative conditions is performed by means of a design of experiments (DoE) with 360 cases of study, as shown in Figure 9. Driving cycle simulations with 36 operative conditions showed fuel consumption and emissions variations below 3% compared to simulations using the 54 experimental calibrated points. So, this approach was selected to reduce the computational time for the e-components calibration. The target for all the configurations was to achieve the same Intake Valve Closing (IVC) conditions than the DMDF HP+LP EGR experimental calibration. This allows to suppose that the combustion process will be the same between the different configurations. Each operating point is tested with 10 blades positions. The maximum powers of both truck platforms are represented in dashed line in Figure 9.

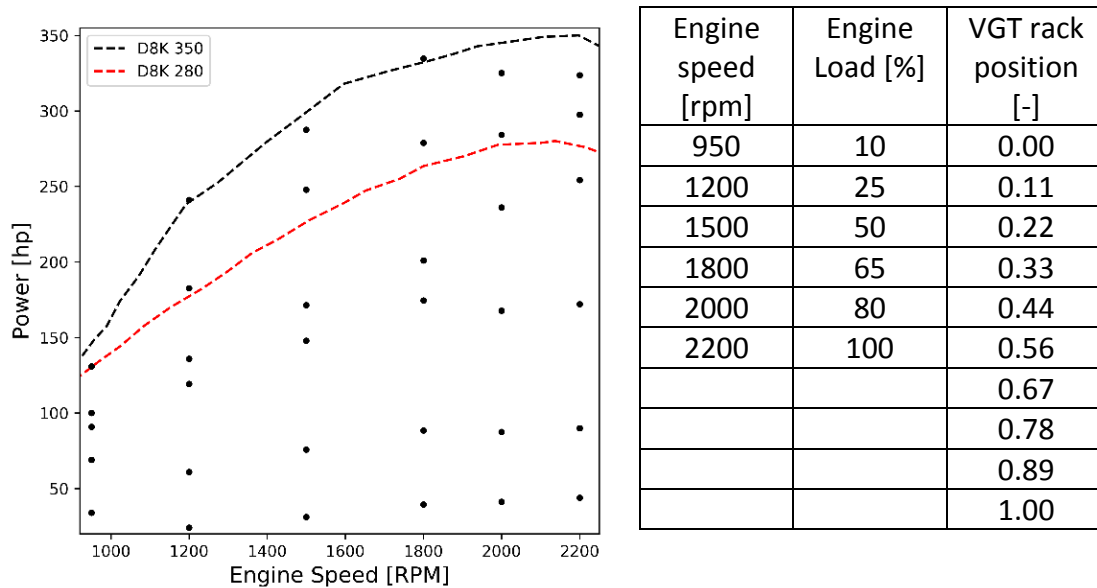| Engine speed [rpm]	Engine Load [%]	VGT rack position [-]
950	10	0.00
1200	25	0.11
1500	50	0.22
1800	65	0.33
2000	80	0.44
2200	100	0.56
		0.67
		0.78
		0.89
		1.00

Figure 9- Engine calibration map with the 36 operative points and test matrix for e-components calibration with ten VGT rack positions discretized from fully-closed to fully-open. The power limit for the two trucks platforms is included in dashed line.

2.3. Vehicle numerical model

The 0-D vehicle model was developed in the GT-Suite for two truck platforms with 18 and 25 ton of maximum payload. These trucks are representative of the European medium-duty sector for goods transportation in urban and extra-urban conditions. Table 2 depicts the main vehicle specifications. The trucks are named as FL (18-ton max payload) and FE (25-ton max payload) and they are originally equipped with the same diesel no-hybrid powertrain but in two power versions: 280 hp and 350 hp as previously mentioned. The calibration is the same with a fuel cut in the upper part of the map for the FL 18-ton version.

Table 2 – Main vehicle specifications for 0-D vehicle model.

Parameter	FL 18-ton truck	FE 25-ton truck
Vehicle model [-]		
Base vehicle Mass [kg]	5240	7035
Max Payload [kg]	12760	17965
Vehicle Drag Coefficient [-]	0.65	
Frontal Area [m^2]	5.52	6.89
Rolling friction [-]	0.0155	
Tires Size [mm/%/inch]	275/80/22.5	295/80/22.5
Gear Box [-]	6 gears	12 gears
Differential ratio [-]	5.29	3.08
ICE rated power [hp]	280$_{@2100rpm}$	350$_{@2200rpm}$

ICE rated Torque [Nm]	1050	1400

The new powertrain model so-called as P0 mild hybrid electric truck model adds a 48V battery pack system and a BAS [35] plus the e-components. The resistive forces (aerodynamic, friction, road slope, etc.) for both truck platforms were validated with on-road measurements with the commercial non-hybrid version as presented in a previous work [32]. The main reasons to select a P0 architecture was due to the need of small changes compared to the original powertrain [36] and the possibility to drive the e-TC and e-EGR pump. It is important to note that, as well as the ICE, the e-components are modelled by means of a map-based approach.
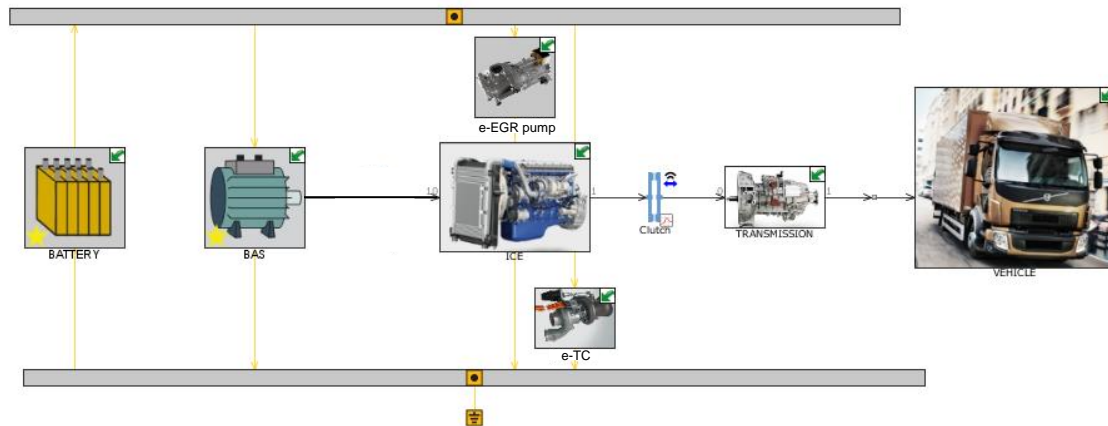

Figure 10- 0D vehicle model for 48V mild hybrid P0 truck with the belt alternator starter (BAS), e-TC and e-EGR pump.

The energy management is the crucial point in hybrid powertrains. For this case, a rule-based controller (RBC) strategy is used [37]. The main parameters defined are the gear shift strategy, battery state of the charge (SOC) above which the BAS assists with the maximum power, vehicle speed below which the BAS assists with the half of the maximum power and minimum battery SOC in which the battery needs to be re-charged [38]. These four parameters are calibrated in homologation conditions (WHVC and 50% of payload) with a design of experiment with 800 cases distributed by a Latin Hypercube type. After the optimum is selected, the vehicle is evaluated under other three driving cycles representative of real drive conditions. Three payload conditions are tested with 0% (empty truck), 50% (homologation condition) and 100% (full truck). Appendix B shows the speed versus time traces of these driving cycles.

3. Results and discussion

The results are organized in four subsections. The subsection 3.1 shows the effects of running the DMDF concept with only HP-EGR, with each individual e-component and with both e-components. The target for all the configurations was to achieve the same Intake Valve Opening (IVC) conditions than the DMDF HP+LP EGR calibrated experimentally. This allows to suppose that the combustion process will be the same between the different configurations. The six most representative engine operative conditions are studied in this subsection. The best case is selected considering the advantages in terms of $BSFC_{eq}$. The subsection 3.2 shows the optimum setup in the complete calibration map (36 operative points) with a detailed view of the effect of changing the VGT position on the energy recovery and air management targets. The

subsection 3.3 analyses the results when both e-components are working simultaneously in terms of fuel consumption benefits and power requirements in all the engine map. The optimum VGT position is selected to achieve the minimum $BSFC_{eq}$. Lastly, the subsection 3.4 shows the effect of using e-components in a P0 MHEV powertrain over four driving conditions and three payloads against the CDC ICE and DMDF ICE configurations.

3.1. e-components selection

Each e-component have a specific objective in the air management strategy. However, the e-TC and e-EGR pump have an effect in each other, making the calibration process a difficult task. In this sense, the study of both components separately and together helps to understand the potential to improve the fuel economy and their effect on the boost pressure and EGR rate. Figure 11 shows the intake pressure and EGR rate when the VGT position is varied from almost closed (VGT=0) to totally open (VGT=1) at 1500 rpm. The target of the DMDF ICE with HP-EGR and LP-EGR is depicted in dashed line.

The use of the e-EGR pump allows to achieve the desired EGR rate in all conditions. Operating alone, or together with the e-TC, the target EGR rates (>30%) are achieved in all the VGT positions even for the 80% engine load operating point , which is a more severe condition due to the high boost pressure required. In this case, the e-EGR pump has a more stable EGR rate than the standard HP EGR systems, which controls the EGR rate by means of a throttle.

However, looking at the boost pressure, the e-TC is fundamental to achieve the desired boost pressure with large VGT opening positions. In the case of using only the HP EGR system and only the e-EGR pump, the boost pressure decays due to the lack of energy in the turbine. For 50% of engine load, the boost pressure is maintained for all the VGT range. On the other hand, for 80% engine load, the e-TC allows to maintain the desired boost pressure up to a VGT position of 0.56. However, for both engine loads, using only the e-TC does not allow to meet the EGR rate for VGT positions higher than 0.2. This is due to the not favourable pressure difference in the HP EGR line. The combination of both e-components allows to achieve both targets in almost all the VGT range. Only at 80% engine load the boost pressure decays due to a limitation in the maximum e-TC power. Therefore, the use of both components together seems to be the best solution to achieve high intake pressures (>2.0 bar) and EGR rates (>30%) in a large range of VGT positions with only a line of HP-EGR .
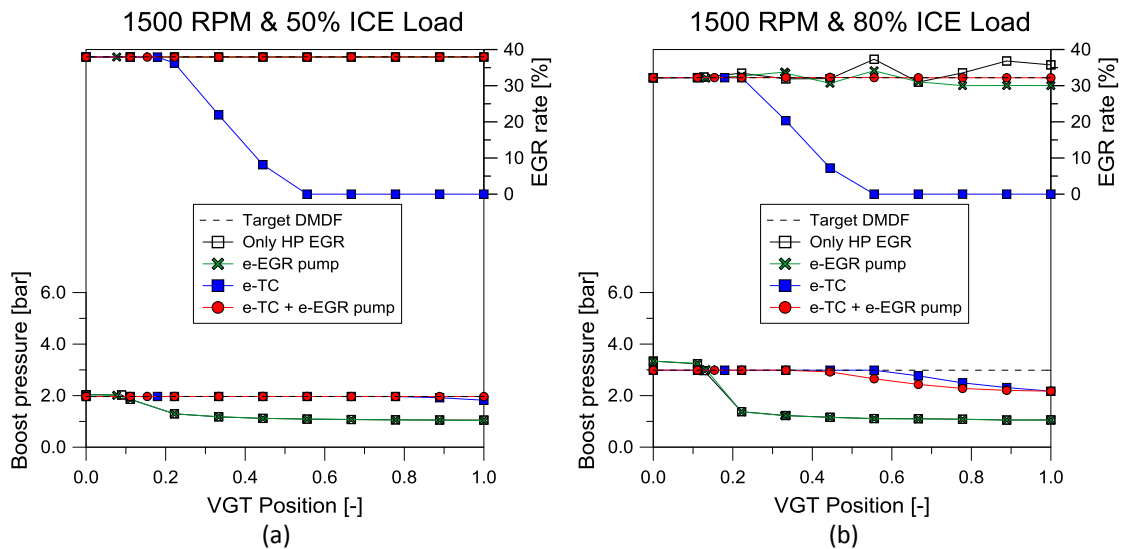
Figure 11- VGT rack position sweep at 1500 rpm and 80% engine load for the case of only HP-EGR, e-EGR pump, e-TC and both e-components together. The results show the response in terms of calibration targets (boost pressure and EGR rate) (a) and turbine inlet conditions (temperature and pressure) (b) for the different configurations.

Figure 12 shows the fuel consumption with respect to the DMDF ICE for those points that meet both targets (boots pressure and EGR rate) in Figure 11. In this sense, is possible to observe that the combined use of the e-TC and the e-EGR pump allows achieving the largest amount of valid points. At 80% of engine load, only one condition for HP EGR and e-EGR pump is possible. The results show penalties in terms of fuel consumption with respect to the reference (HP+LP EGR case) in all cases, with the lower $BSFC_{eq}$ increase found with the e-TC + e-EGR pump. The main reasons for not improving the $BSFC_{eq}$ with respect to the baseline case are the high simultaneous EGR and boost pressure requirement with low possibilities of energy recovery, and that the combustion process was optimized for the HP+LP EGR strategy in these specific points.
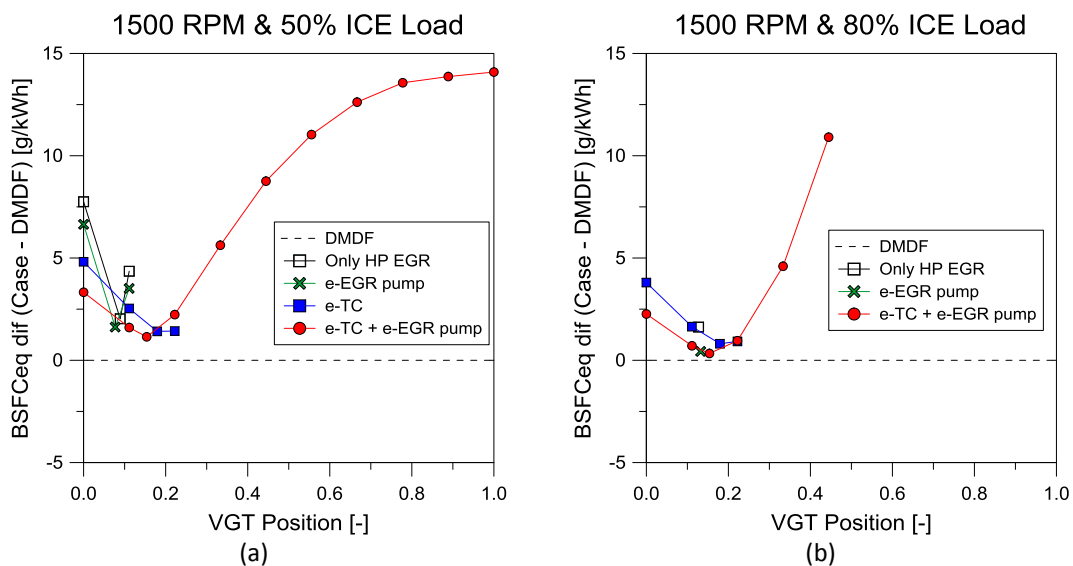

Figure 12- Equivalent brake specific fuel consumption for different VGT rack positions at 1500 rpm and 80% engine load that achieve the baseline calibration targets and do not exceed the turbine inlet limits for the cases of only HP-EGR, e-EGR pump, e-TC and both e-components together.

The same approach was done for other two engine rotational speeds (1200 and 1800). The results in Figure 13 shows that the reduction of the engine speed helps to the new setup to improve with respect to the baseline. In addition, the strategy of using only HP-EGR shows the worst results in terms of $BSFC_{eq}$ and does not allow to achieve the targets at 1200 rpm and 50% load. At 50% engine load, the e-EGR pump has worse $BSFC_{eq}$ than the e-TC. This trend is reverted for 80% engine load, with the case of using only the e-EGR pump close to the case of using both e-components. This is mainly due to the calibration targets requirements and the energy available in the turbine. At medium engine load, the energy in the turbine is lower than at high engine load. In addition, the DMDF calibration uses high EGR rate (≈40%), decreasing even more the turbocompounding energy. Therefore, the turbine blades need to be closed to achieve the desire boost pressure. In this case, the use of an e-TC is beneficial to reduce the pumping losses by delivering power through the electric motor. In the case of high engine load, more energy is available due to the energy in the combustion process and less EGR rate demanded (≈30%). Therefore, the e-TC is not beneficial as at 50% engine load. In this sense, when the load increases, the EGR rate decreases due to excessive soot emissions and the boost pressure increases to achieve the engine power required.

From these results, it is concluded that the use of both components simultaneously is the best option when the LP-EGR line is removed in a DMDF combustion mode. Therefore, the next section analyzes the performance of this configuration in all the engine map.
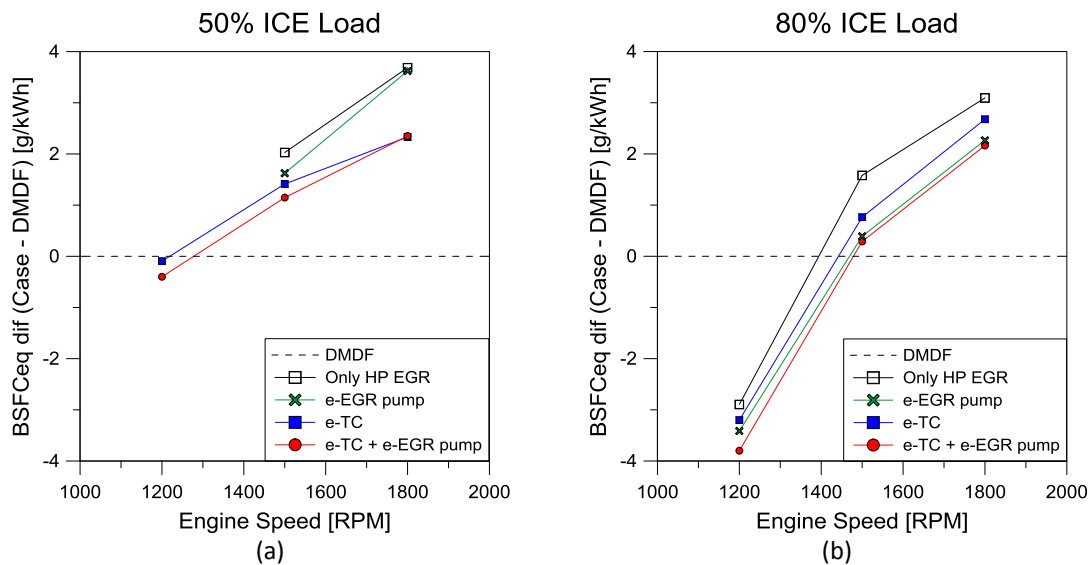

Figure 13- Equivalent brake specific fuel consumption for different VGT rack positions at 50% and 80% engine load for the cases of only HP-EGR, e-EGR pump, e-TC and both e-components together.

3.2. e-TC & e-EGR pump trends

Figure 14 shows the effect of varying the turbine rack position over the e-TC (Figure 14a) and e-EGR pump (Figure 14b) energy power for six engine speed and engine loads. Positive power means energy delivered from the shaft of each component to the gas flow and negative means energy recovered from the gas flow. In spite of that these results represent the behaviour in stationary conditions, they are obtained after several iteration cycles in which the control system adjusts the e-TC power and e-EGR pump

speed to achieve the air management targets (EGR rate, intake pressure and in-cylinder temperatures). The simulation is stopped after the settings are between the 2% of the target. Open the VGT means that the e-TC needs to deliver more power because less energy is taken by the turbine blades. This reduces the exhaust backpressure just before the engine-out pipe, where the HP EGR line is located. Therefore, the e-EGR pump needs also to deliver power to achieve the desired EGR target. In spite of this seems to be a disadvantage, the pumping means effective pressure (PMEP) is also reduced (Figure 14c) increasing the engine brake power. It is interesting to note that engine loads greater than 25% do not have results for all the VGT positions because they exceeded the turbine limits. The analysis of the other five engine rotational speeds are included in the appendix C.
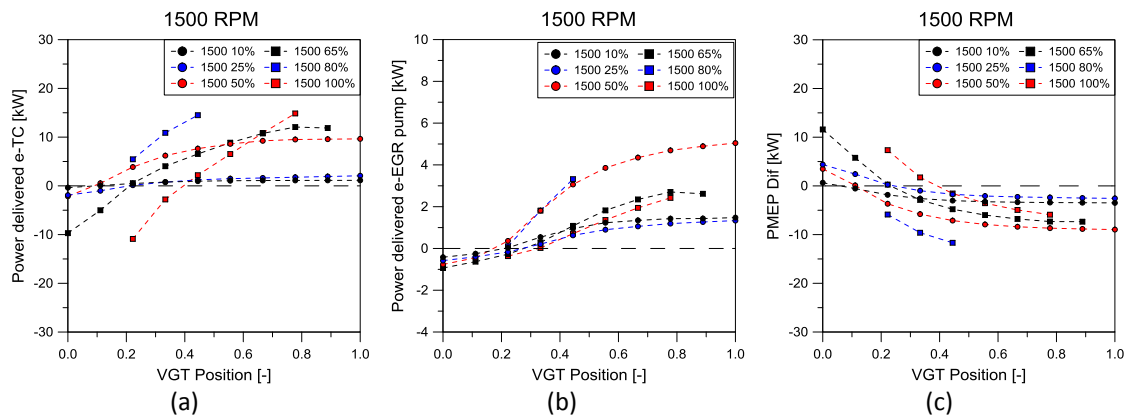

Figure 14- Power delivered/recovered by the e-TC (a), power delivered/recovered by the e-EGR pump (b) and pumping mean effective pressure difference with respect to the DMDF LP+HP EGR calibration (c) for different VGT rack positions at 1500 rpm .

Figure 15 shows the results for all the cases at 1500 rpm and 80% of engine load. When the VGT rack position is below 0.1, the turbine inlet pressure exceeds the mechanical safety limit imposed at 3.8 bar. Pasini et al [10] noted the importance of choosing a turbine characterized by a flow capacity large enough to avoid high backpressure penalties, even if slight or no effect on fuel consumption occurs. However, the change of turbine geometry is out of the scope of the current work. On the other hand, when the VGT rack position is higher than 0.4, the turbine inlet pressure is below 2% of the target. The main reason for this is that the e-TC power demand exceeds the maximum value of 15 kW. Therefore, the e-TC cannot achieve the boost pressure required at this operating condition. In spite of the possibility to increase the electric machine maximum power of the e-TC to achieve the desired boost pressure, Figure 14c not show improvements in terms of PMEP in this zone. Therefore, this zone does not represent a potential benefit to reduce the fuel consumption.
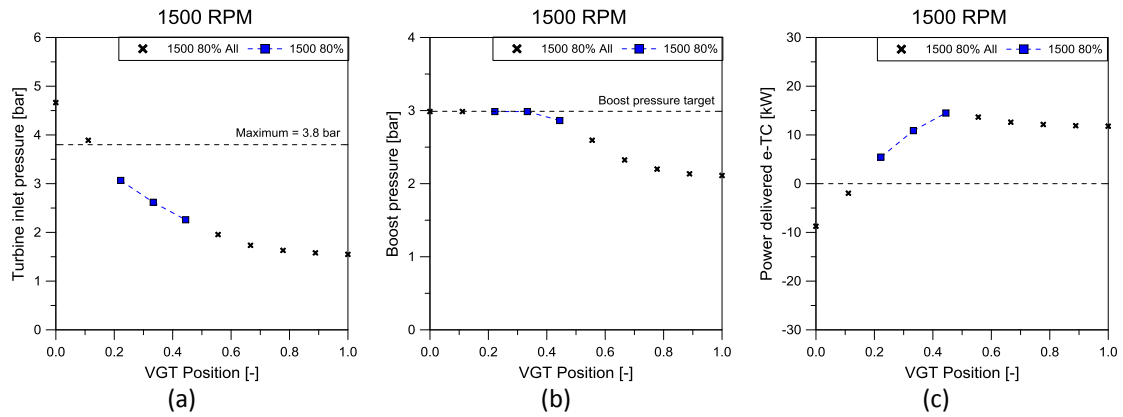
Figure 15 - Power delivered by the e-TC (a), turbine inlet pressure (b) and boost pressure (c) at 1500 rpm and 80% engine load for different VGT rack positions.

Finally, the total power is calculated as the sum of the brake power (mainly affected by the PMEP change) and the electrical power of the e-components. Then, the new $BSFC_{eq}$ is calculated considering the same fuel injection than the original DMDF ICE calibration. Figure 16 shows the results for both abovementioned parameters with the optimum marked with a star. From the $BSFC_{eq}$ trend, it is possible to identify the engine loads that have limitations to achieve the targets and the increase of the engine efficiency with the engine load increase. For all the cases, the optimum values are found for VGT positions below 0.4 and decrease with the engine load increase. The maximum engine load (100%) has larger operative range than 80% load due to the lower EGR rates required in the DMDF ICE calibration (see Figure 1a).
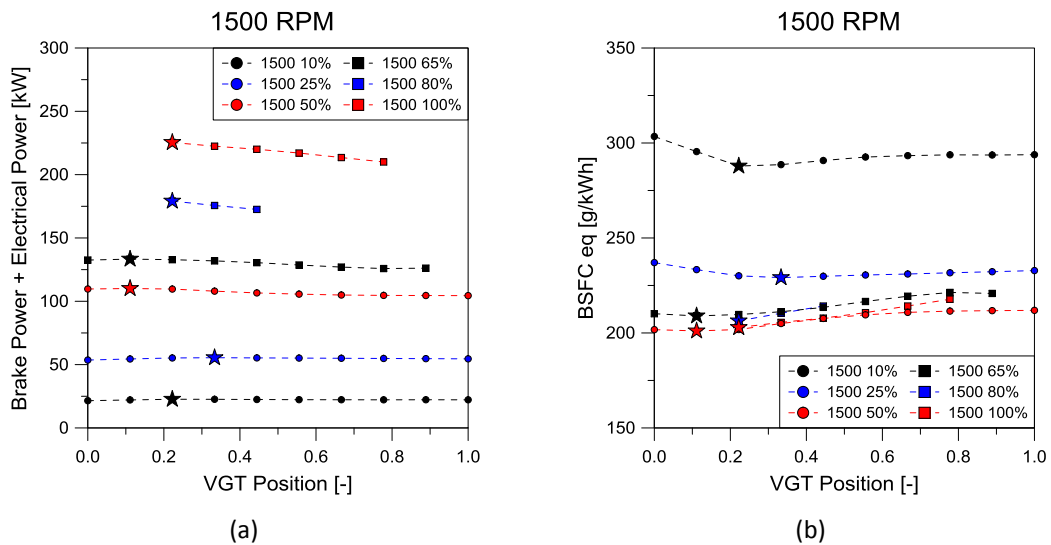

Figure 16 – Total power (a) and equivalent brake specific fuel consumption for different VGT rack positions at 1500 rpm and different engine loads.

3.3. e-Components calibration maps

All the optimum operative conditions for the e-TC and e-EGR are obtained and plotted as an interpolation map for different parameters in this section. Figure 17 shows the e-TC and e-EGR pump power requirements in all the operative conditions. The e-TC power ranges from 6 kW in motor and -15 kW as generator. Therefore, the sizing of the original planned motor (15 kW) is selected correctly. In addition, the e-EGR pump shows

low power requirements with 0.5 kW in motor and -1.0 kW in generator. The speed set up for each e-component is shown in Figure 18. This is a crucial parameter for the design, and it can be useful in future components developments.
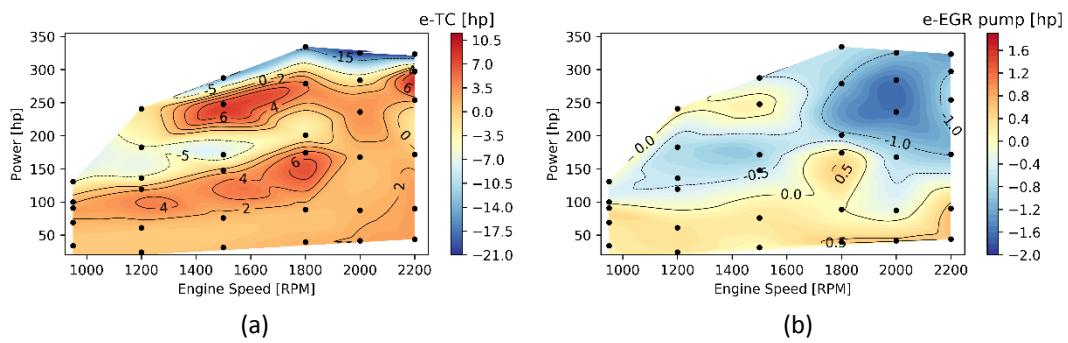

(a)

(b)

Figure 17 – Power calibration maps for the e-TC (a) and e-EGR pump (b) working together to achieve the same calibration targets than the DMDF LP+HP EGR calibration.
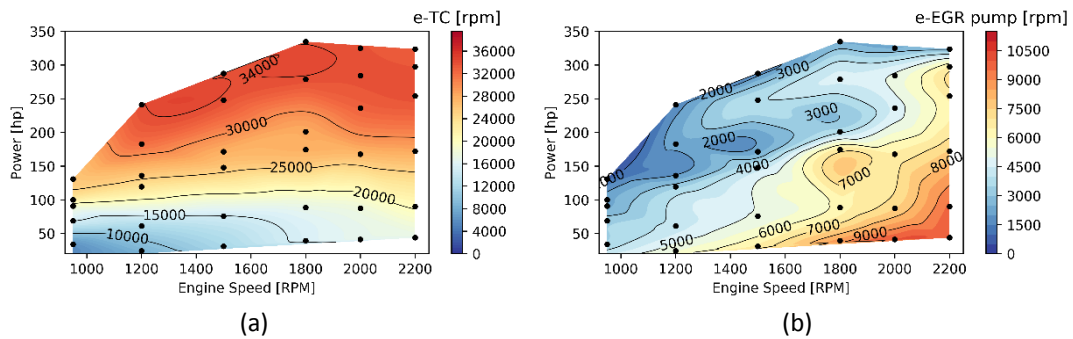

(a)

(b)

Figure 18 – Rotational speed maps for the e-TC (a) and e-EGR pump (b) working together to achieve the same calibration targets than the DMDF LP+HP EGR calibration.

The VGT position final results and pumping work are shown in Figure 19. The VGT is generally near to the minimum position (close to 0.1) at low rotational speed and high rotational speed close to 0.33 (see Figure 19a). Therefore, this generates an increase of the pumping work at middle engine load zones, as shown in Figure 19b. The major benefits are found at low engine loads, where the VGT was almost closed in the original calibration to achieve the desired boost pressure.
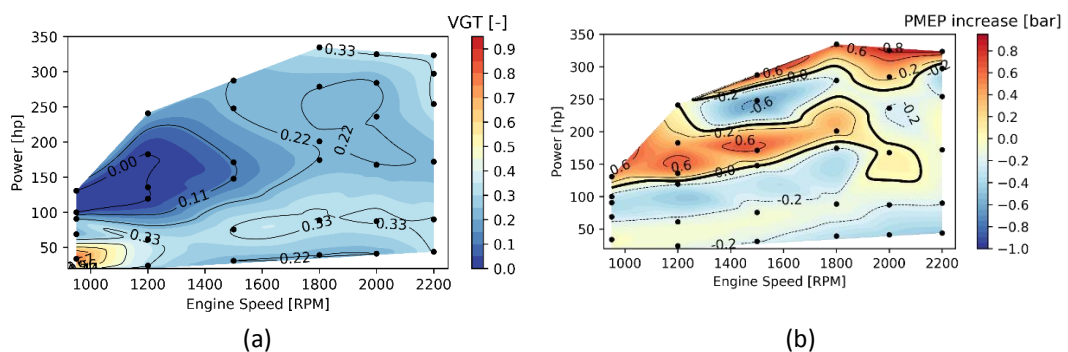

(a)

(b)

Figure 19 – Calibration maps of the VGT rack position (a) and pumping mean effective pressure difference versus the DMDF LP+HP EGR calibration (b).

In a first step, the equivalent brake specific fuel consumption is plotted to quantify the gains with respect to the DMDF ICE (Figure 20a) and CDC calibration (Figure

20b). Figure 21a shows close BSFC values at medium and high loads (around ±2 g/kWh), with the major benefits from the use of the e-components found at low load and high engine speed, where up to 50 g/kWh improvement is achieved. This zone allows to recovery energy with the e-TC and reduce PMEP due to the turbine rack position. In this zone, the DMDF calibration is limited due to hardware restrictions. Figure 21b shows that the optimum zone when comparing to the CDC calibration is around 1500 rpm and 120 hp, similar to the results shown in Figure 3. At low loads, the new calibration is close to the CDC values, totally different to the trend found with the DMDF configuration. It is important to remark that the new calibration not only achieves similar or better results in terms of BSFC, but also avoids the use of a LP-EGR system to obtain the same emissions than the DMDF calibration, which was proposed as one of the main targets for this work. In spite of the improvements achieved by the DMDF concept in terms fuel consumption, it is clear that a new turbine design is needed due to the small part used of the current turbine geometry (below 40% of the turbine possibilities).

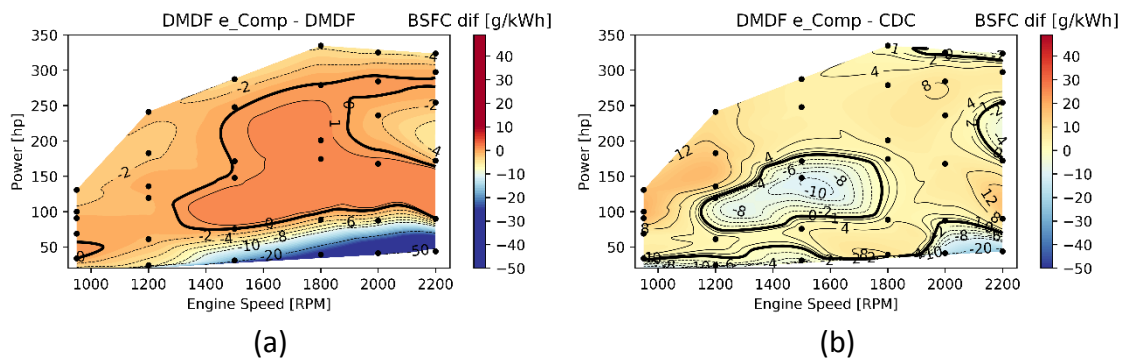(a)   (b)

Figure 20 – Brake specific fuel consumption of the DMDF e-components calibration against DMDF HP+LP EGR (a) and CDC (b) calibration maps.

3.4. Effect in driving cycles

To quantify the potential of using e-components in real truck operation conditions, a 0D vehicle numerical model is used to simulate different driving cycles. To simulate the behavior of the engine operation with the 48 V e-components system, the real BSFC engine map and the maps for the e-components (Figure 17) are used to simulate the power requirements in the battery. It is important to note that this approach considers the battery losses due to charge and discharge events of the e-components. Therefore, a close scenario to real operation can be studied. The BAS is also included to simulate the start-stop and brake energy recovery along the cycles. This component is fundamental for the re-charge of the battery. For brevity of the manuscript, the instantaneous values are only presented for the FL 18-ton truck at homologation conditions (WHVC and 50% payload), while Figure 24 and Figure 25 summarize the final results for both trucks in all the simulated conditions.

Figure 21 shows the engine speed- time and torque- time profiles for the two powertrains analyzed (non-hybrid CDC and mild hybrid P0 DMDF with e-components). The non-hybrid DMDF and P0 DMDF HP+LP EGR powertrains are not included for similarities with the previous cases. As it can be seen, the engine speed is higher for the non-hybrid CDC powertrain due to the larger gear shift strategy. To achieve the same total power at the wheels, the P0 DMDF with e-components powertrain needs to deliver

higher engine torque. Figure 22a show the BAS operation, with positive values representing power delivery to the engine and negative values meaning energy regeneration (or battery charging) from the engine. The operation has pulsed behavior with power peaks up to 30 hp (maximum BAS power) and -30 hp in braking conditions. Figure 22b depicts the system voltage around 48v and the e-TC and EGR-pump power consumption. Both e-components have energy consumption from the battery (negative power values), with the e-TC having greater consumption than the e-EGR (as anticipated in Figure 17). For both cases, the peak power consumption is lower than that of the BAS, so that the e-components do not have a large influence on the battery size and electric components selections.
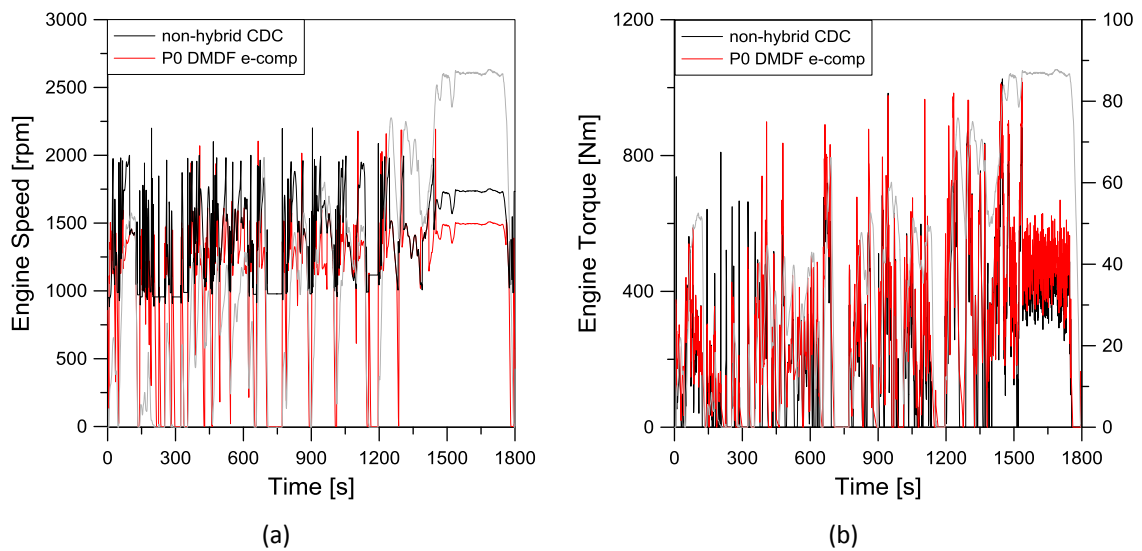

(a) (b)

Figure 21 – Engine speed (a) and engine torque (b) for the non-hybrid CDC and the P0 DMDF with e-components cases in homologation conditions. The WHVC driving cycle speed profile is added in the background for reference.
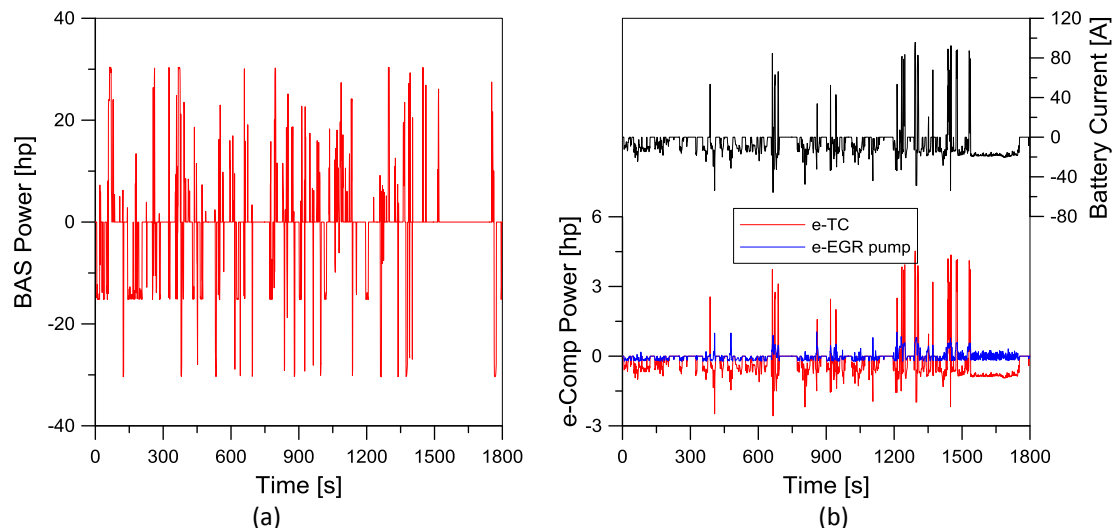

(a) (b)

Figure 22 – Belt assist starter power (a) and e-components voltage and power (b) for the P0 DMDF with e-components case in homologation conditions.

The cumulative fuel consumption and NOx emissions for all the powertrains considered in this work are depicted in Figure 23. Figure 23a show that the DMDF P0 with and without e-components achieves similar final fuel consumption, with a

considerable reduction of the fuel consumption in the urban part of the WHVC as compared to the other two vehicle architectures. In the rural and highway phases, no great differences are found in fuel consumption, but they allow to reduce the total fuel consumption with savings of CO_2 emissions around 5% with respect to the CDC non-hybrid case at the end of the cycle. The cumulative engine-out NOx emissions (Figure 23b) are strongly reduced due to the DMDF operation. Both the mild hybrid and non-hybrid DMDF powertrains allow reducing the NOx emissions more than 90% with respect to the CDC. These results allow to estimate that the SCR-urea ATS would be not necessary in the DMDF cases.
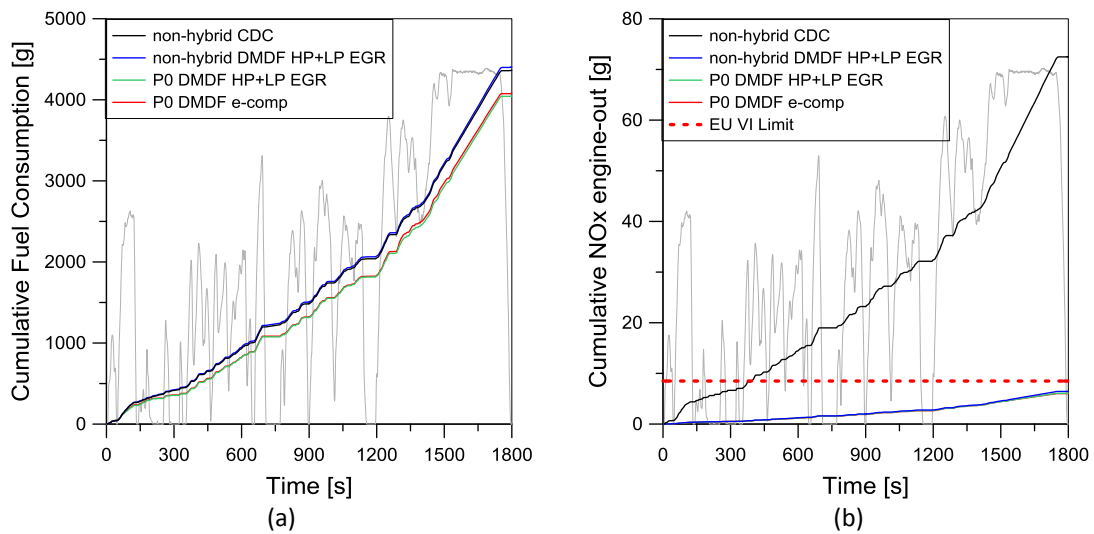

Figure 23 – Cumulative fuel consumption (a) and cumulative NOx engine-out emissions for the four cases studied in homologation conditions. The WHVC driving cycle speed profile is added in the background for reference.

The global results for the two trucks in all the driving conditions are presented in Figure 24 and Figure 25. The results show that the e-components do not improve the fuel economy of the smaller truck with respect to the DMDF HP+LP EGR in a P0 architecture, especially when employed at medium and high payload. As the FL 18-ton truck uses the de-rated map, 100% engine load zone shown in Figure 20, that has up to 4 g/kWh of fuel consumption improvement, it is not used. Therefore, the medium zone (150 hp and 1600 rpm) is mostly used for 50% and 100% payload. In the case of the empty truck, the low load engine map zone is used, in which the fuel consumption is improved up to 30 g/kWh.

The e-components layout is much more advantageous in the case of the larger vehicle, particularly when extra-urban roads or motorways are considered. In fact, under these conditions, the engine works mainly in the high loads and speed region and consequently the e-components recovered significantly larger electrical power that causes a fuel consumption improvement. In addition, the FE 25-ton does not have penalties at full payload as the FL 18-ton thanks to the usage of the 80-100% engine load zone.

For both trucks, the improvement in homologation conditions (WHVC and 50% payload) achieves 6.0% of fuel improvement versus CDC in conventional powertrain. This means that similar CO_2 reductions can be achieved, giving to the proposed technology the opportunity to remove LP EGR line, and reduce the DPF size and regeneration times. However, it is necessary an experimental campaign to perform particle number measurements. This is expected in future works.
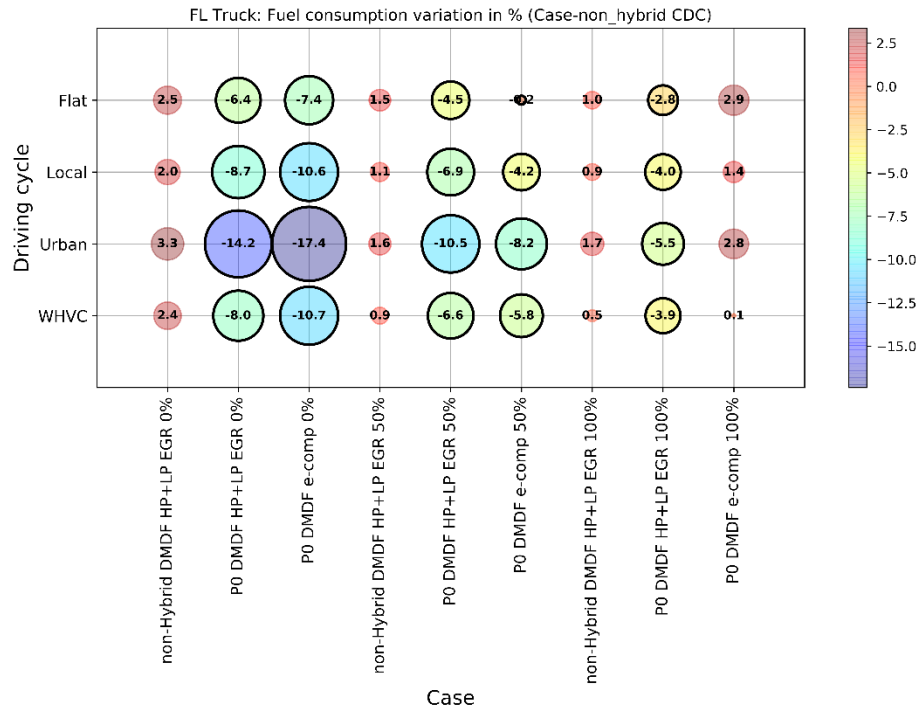

Figure 24 – Summary of the results for the FL truck in terms of total fuel consumption difference against the non-hybrid CDC along the WHVC, Urban, Local and Flat cycles at 0%, 50% and 100% payloads.
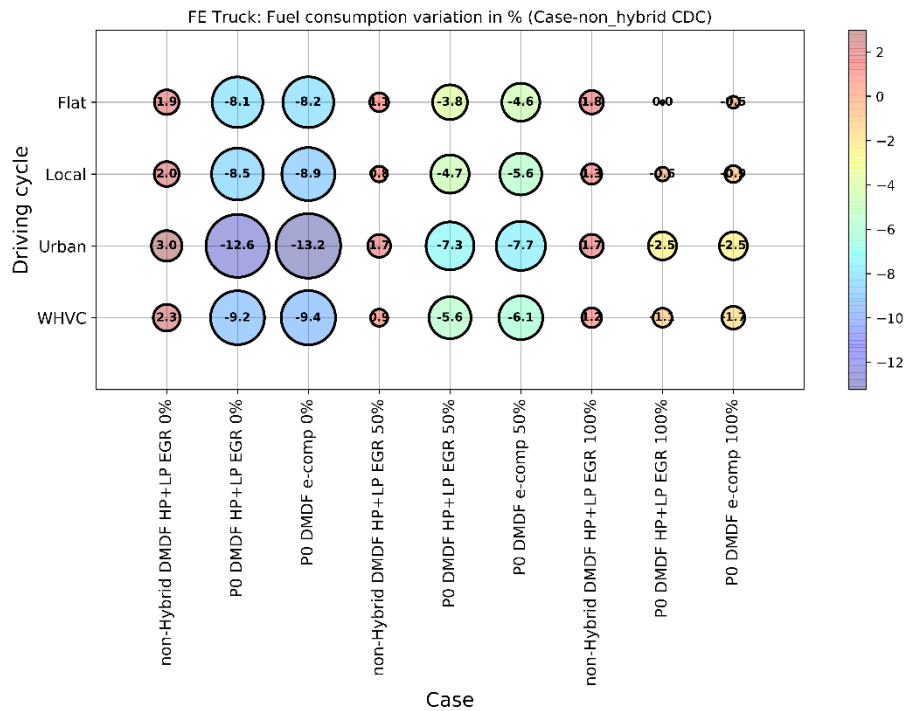
Figure 25 - Summary of the results for the FE truck in terms of total fuel consumption difference against the non-hybrid CDC along the WHVC, Urban, Local and Flat cycles at 0%, 50% and 100% payloads.

4. Conclusions

The evaluation of electric turbocompounding and electric EGR pump was performed by numerical simulations with a 0D vehicle model. The 48 V electric components were used to achieve the same air management targets than a high-pressure/low pressure system in a low temperature combustion mode. The only use of HP EGR was proposed to reduce the engine packaging and improve the transient behavior. The results show that the only use of HP EGR does not allow to achieve all the calibration points of the engine and increases the fuel consumption. The introduction of the e-components allows to work in an extended range of VGT rack positions. The optimum case was with both e-components working together.

All the calibration map studied with both e-components shows improvements of fuel consumption at extreme cases: low engine rotational speed, low engine load or maximum engine load. All the cases where energy recovery can be done and the baseline case has difficulties for the well operation.

Lastly, two medium-duty truck platforms were tested with a mild hybrid P0 powertrain. The new e-component calibration (P0 DMDF e-comp) was compared against the non-hybrid CDC, non-hybrid DMDF HP+LP EGR and P0 DMDF HP+LP EGR The results show that P0 allows advantages over the non-hybrid architecture between 2% (high payload and large highway phases) and 17% (low payload and large urban phases). The e-components show improvements with respect to the non-hybrid DMDF HP+LP EGR in low payload conditions.

Abbreviations

ATS	Aftertreatment systems	hp	Horse Power
BEV	Battery electric vehicles	HP-EGR	High pressure EGR
BMEP	Brake mean effective pressure	ICE	Internal combustion engine
BSCO	Brake specific CO emissions	LD	Light Duty
$BSCO_2$	Brake specific CO_2 emissions	LI-Ion	Lithium Ion batteries
BSFC	Brake specific fuel consumption	LP-EGR	Low pressure EGR
BSHC	Brake specific HC emissions	LTC	Low temperature combustion
BSNOx	Brake specific NOx emissions	MD	Medium Duty
BSSoot	Brake specific soot emissions	MHEV	Mild hybrid electric vehicle
CDC	Conventional diesel combustion	NOx	Nitrogen Oxides
CI	Compression Ignition	OEM	Original equipment manufacturer
CO	Carbon Monoxide	P0	Belt alternator starter hybrid powertrain
CR	Compression ratio	P1	Parallel hybrid electric vehicle without clutch
DI	Direct Injection	P2	Parallel hybrid electric vehicle pre-transmission
DMDF	Dual mode dual fuel	P3	Parallel hybrid electric vehicle pos transmission
DOC	Diesel Oxidation Catalyst	PHEV	Plug in electric vehicle
DoE	Design of Experiments	PM	particle matter
DPF	Diesel particle filter	PN	Particle number
e-ATS	Electric heater aftertreatment systems	RBC	Rule base control
EBTG	electric-booster and turbo-generator system	RCCI	Reactivity Controlled Compression Ignition
e-EGR Pump	Electric pump for exhaust gas recirculation	rpm	Revolution per minute
EGR	Exhaust gas recirculation	SCR	Selective Catalytic Reduction
EM	Electric motor	SI	Spark Ignition
EU	European Union	SOC	State of the charge of the battery
FCEV	fuel cell vehicles	tkm	ton per kilometer
FHEV	Full hybrid vehicle	TM	Traction Motor
GEN	Generator Motor	TTW	Tank to wheel
GHG	greenhouse gas emissions	VGT	Variable-geometry turbine
HC	Unburned Hydrocarbons	WHRS	Waste-heat recovery systems
HCCI	Homogeneous charge compression ignition	WHVC	World Harmonized Vehicle Cycle
HD	Heavy Duty	WTW	Well to wheel
HEV	Hybrid electric vehicle	ZEV	Zero Emission Vehicles

References

[1]   A. Jain, T. Nueesch, C. Naegele, P. M. R. Lassus, and C. H. Onder, "Modeling and Control of a Hybrid Electric Vehicle with an Electrically Assisted Turbocharger," *IEEE Trans. Veh. Technol.*, vol. 65, no. 6, pp. 4344–4358, 2016.

[2]   A. García, J. Monsalve-Serrano, S. Martínez-Boggio, V. Rückert Roso, and N. Duarte Souza Alvarenga Santos, "Potential of bio-ethanol in different advanced combustion modes for hybrid passenger vehicles," *Renew. Energy*, vol. 150, pp. 58–77, May 2020.

[3]   Official website of the European Union, "Reducing CO2 emissions from heavy-duty vehicles," *2020*. [Online]. Available: https://ec.europa.eu/clima/policies/transport/vehicles/heavy_en. [Accessed: 09-Nov-2020].

[4]   A. Joshi, "Review of Vehicle Engine Efficiency and Emissions," *SAE Tech. Pap.*, vol. 2020-April, no. April, pp. 1–29, 2020.

[5]   V. Bermúdez, A. García, D. Villalta, and L. Soto, "Assessment on the consequences of injection strategies on combustion process and particle size distributions in Euro VI medium-duty diesel engine," *Int. J. Engine Res.*, vol. 21, no. 4, pp. 683–697, 2020.

[6]   N. Sulaiman, M. A. Hannan, A. Mohamed, P. J. Ker, E. H. Majlan, and W. R. Wan Daud, "Optimization of energy management system for fuel-cell hybrid electric vehicles: Issues and recommendations," *Appl. Energy*, vol. 228, no. July, pp. 2061–2079, 2018.

[7]   W. Zhuang *et al.*, "A survey of powertrain configuration studies on hybrid electric vehicles," *Appl. Energy*, vol. 262, no. February, p. 114553, 2020.

[8]   A. P. Vora *et al.*, "Design-space exploration of series plug-in hybrid electric vehicles for medium-duty truck applications in a total cost-of-ownership framework," *Appl. Energy*, vol. 202, pp. 662–672, 2017.

[9]   M. Preißinger, J. A. H. Schwöbel, A. Klamt, and D. Brüggemann, "Multi-criteria evaluation of several million working fluids for waste heat recovery by means of Organic Rankine Cycle in passenger cars and heavy-duty trucks," *Appl. Energy*, vol. 206, no. August, pp. 887–899, 2017.

[10]   G. Pasini *et al.*, "Evaluation of an electric turbo compound system for SI engines: A numerical approach," *Appl. Energy*, vol. 162, pp. 527–540, 2016.

[11]   Q. Hu *et al.*, "Engine and Aftertreatment Co-Optimization of Connected HEVs via Multi-Range Vehicle Speed Planning and Prediction," *SAE Tech.*, vol. 01, p. 0590, Apr. 2020.

[12]   EATON, "Diesel engine EGR pump," 2020. [Online]. Available: https://www.eaton.com/us/en-us/products/engine-solutions/superchargers/TVS-technology-applications/tvs-diesel-egr-pump.html. [Accessed: 09-Nov-2020].

[13] F. Graf, S. Lauer, J. Hofstetter, and M. Perugini, "Optimal Thermal Management and Electrification in 48-V Hybrids," *MTZ Worldw.*, vol. 79, no. 10, pp. 38–43, 2018.

[14] A. Shabashevich, N. Richards, J. Hwang, and P. A. Erickson, "Analysis of powertrain design on effective waste heat recovery from conventional and hybrid electric vehicles," *Appl. Energy*, vol. 157, pp. 754–761, 2015.

[15] W. He, R. Guo, S. Liu, K. Zhu, and S. Wang, "Temperature gradient characteristics and effect on optimal thermoelectric performance in exhaust power-generation systems," *Appl. Energy*, vol. 261, no. December 2019, p. 114366, 2020.

[16] D. Zi, L. Zhang, B. Chen, and Q. Zhang, "Study of the electric-booster and turbo-generator system and its influence on a 1.5 L gasoline engine," *Appl. Therm. Eng.*, vol. 162, no. August, p. 114236, 2019.

[17] X. Xue and J. Rutledge, "Potentials of Electrical Assist and Variable Geometry Turbocharging System for Heavy-Duty Diesel Engine Downsizing," *SAE Tech. Pap.*, vol. 2017-March, no. March, 2017.

[18] R. Burke, A. Giedymin, Z. Wu, H. Chuan, N. Bourne, and J. G. Hawley, "A Lumped Parameter Thermal Model for Single-Sided AFPM Machines with Experimental Validation," *IEEE Trans. Transp. Electrif.*, vol. 6, no. 3, pp. 1065–1083, 2020.

[19] A. M. Andwari, A. A. Aziz, M. F. M. Said, and Z. A. Latiff, "Experimental investigation of the influence of internal and external EGR on the combustion characteristics of a controlled auto-ignition two-stroke cycle engine," *Appl. Energy*, vol. 134, pp. 1–10, Dec. 2014.

[20] H. W. Wu, T. T. Hsu, C. M. Fan, and P. H. He, "Reduction of smoke, PM2.5, and NOX of a diesel engine integrated with methanol steam reformer recovering waste heat and cooled EGR," *Energy Convers. Manag.*, vol. 172, no. X, pp. 567–578, 2018.

[21] D. Wang, L. Shi, S. Zhu, B. Liu, Y. Qian, and K. Deng, "Numerical and thermodynamic study on effects of high and low pressure exhaust gas recirculation on turbocharged marine low-speed engine," *Appl. Energy*, vol. 261, no. December 2019, p. 114346, 2020.

[22] J. Park, S. Song, and K. S. Lee, "Numerical investigation of a dual-loop EGR split strategy using a split index and multi-objective Pareto optimization," *Appl. Energy*, vol. 142, pp. 21–32, 2015.

[23] A. García, J. Monsalve-Serrano, D. Villalta, R. Lago Sari, V. Gordillo Zavaleta, and P. Gaillard, "Potential of e-Fischer Tropsch diesel and oxymethyl-ether (OMEx) as fuels for the dual-mode dual-fuel concept," *Appl. Energy*, vol. 253, no. May, p. 113622, 2019.

[24] J. Benajes, A. García, J. Monsalve-Serrano, and R. Lago Sari, "Fuel consumption and engine-out emissions estimations of a light-duty engine running in dual-mode RCCI/CDC with different fuels and driving cycles," *Energy*, vol. 157, pp. 19–30, 2018.

[25]   P. Olmeda, A. García, J. Monsalve-Serrano, and R. Lago Sari, "Experimental investigation on RCCI heat transfer in a light-duty diesel engine with different fuels: Comparison versus conventional diesel combustion," *Appl. Therm. Eng.*, vol. 144, no. August, pp. 424–436, 2018.

[26]   A. García, J. Monsalve-Serrano, D. Villalta, and R. Sari, "Fuel sensitivity effects on dual-mode dual-fuel combustion operation for different octane numbers," *Energy Convers. Manag.*, vol. 201, no. September, p. 112137, 2019.

[27]   J. Benajes, A. García, J. Monsalve-Serrano, and V. Boronat, "Achieving clean and efficient engine operation up to full load by combining optimized RCCI and dual-fuel diesel-gasoline combustion strategies," *Energy Convers. Manag.*, vol. 136, pp. 142–151, 2017.

[28]   S. Molina, A. García, J. Monsalve-Serrano, and D. Villalta, "Effects of fuel injection parameters on premixed charge compression ignition combustion and emission characteristics in a medium-duty compression ignition diesel engine," *Int. J. Engine Res.*, vol. 0, no. 0, p. 146808741986701, Jul. 2019.

[29]   S. Molina, A. García, J. Monsalve-Serrano, and D. Estepa, "Miller cycle for improved efficiency, load range and emissions in a heavy-duty engine running under reactivity controlled compression ignition combustion," *Appl. Therm. Eng.*, vol. 136, no. March, pp. 161–168, 2018.

[30]   J. Benajes, A. García, J. Monsalve-Serrano, and R. Sari, "Clean and efficient dual-fuel combustion using OMEx as high reactivity fuel: Comparison to diesel-gasoline calibration," *Energy Convers. Manag.*, vol. 216, no. March, p. 112953, Jul. 2020.

[31]   A. P. Singh, V. Kumar, and A. K. Agarwal, "Evaluation of comparative engine combustion, performance and emission characteristics of low temperature combustion (PCCI and RCCI) modes," *Appl. Energy*, vol. 278, no. July, p. 115644, 2020.

[32]   A. García, J. Monsalve-Serrano, S. Martinez-Boggio, P. Gaillard, O. Poussin, and A. A. Amer, "Dual fuel combustion and hybrid electric powertrains as potential solution to achieve 2025 emissions targets in medium duty trucks sector," *Energy Convers. Manag.*, vol. 224, no. June, p. 113320, Nov. 2020.

[33]   Gamma Technologies, "GT-Suite," *2020*. [Online]. Available: https://www.gtisoft.com/. [Accessed: 07-Dec-2020].

[34]   H. Dong *et al.*, "Experiment and simulation investigation on energy management of a gasoline vehicle and hybrid turbocharger optimization based on equivalent consumption minimization strategy," *Energy Convers. Manag.*, vol. 226, no. August, p. 113518, 2020.

[35]   R. Finesso, E. Spessa, and M. Venditti, "Layout design and energetic analysis of a complex diesel parallel hybrid electric vehicle," *Appl. Energy*, vol. 134, pp. 573–588, 2014.

[36]   J. Benajes, A. García, J. Monsalve-Serrano, and S. Martínez-Boggio,

"Optimization of the parallel and mild hybrid vehicle platforms operating under conventional and advanced combustion modes," *Energy Convers. Manag.*, vol. 190, no. April, pp. 73–90, Jun. 2019.

[37]   Z. Song, H. Hofmann, J. Li, J. Hou, X. Han, and M. Ouyang, "Energy management strategies comparison for electric vehicles with hybrid energy storage system," *Appl. Energy*, vol. 134, pp. 321–331, 2014.

[38]   H. Marzougui, A. Kadri, J. P. Martin, M. Amari, S. Pierfederici, and F. Bacha, "Implementation of energy management strategy of hybrid power source for electrical vehicle," *Energy Convers. Manag.*, vol. 195, no. February, pp. 830–843, 2019.

Appendix A

(a)

(b)
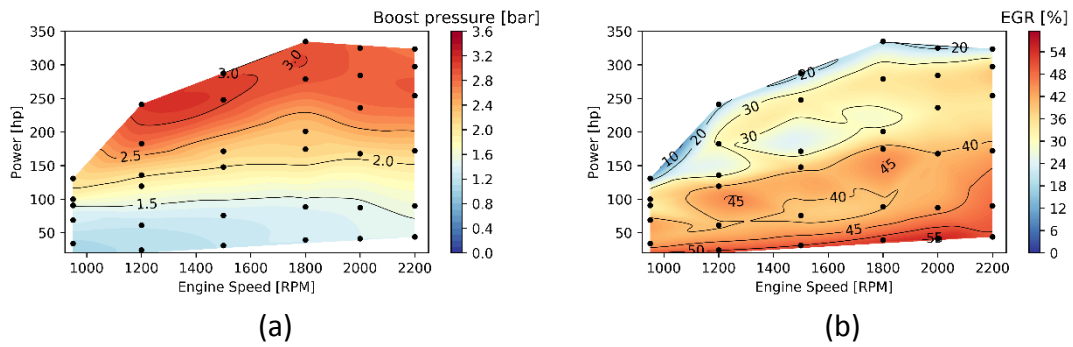
Figure A1- Boost pressure (a) and EGR rate (b) for DMDF ICE configuration.
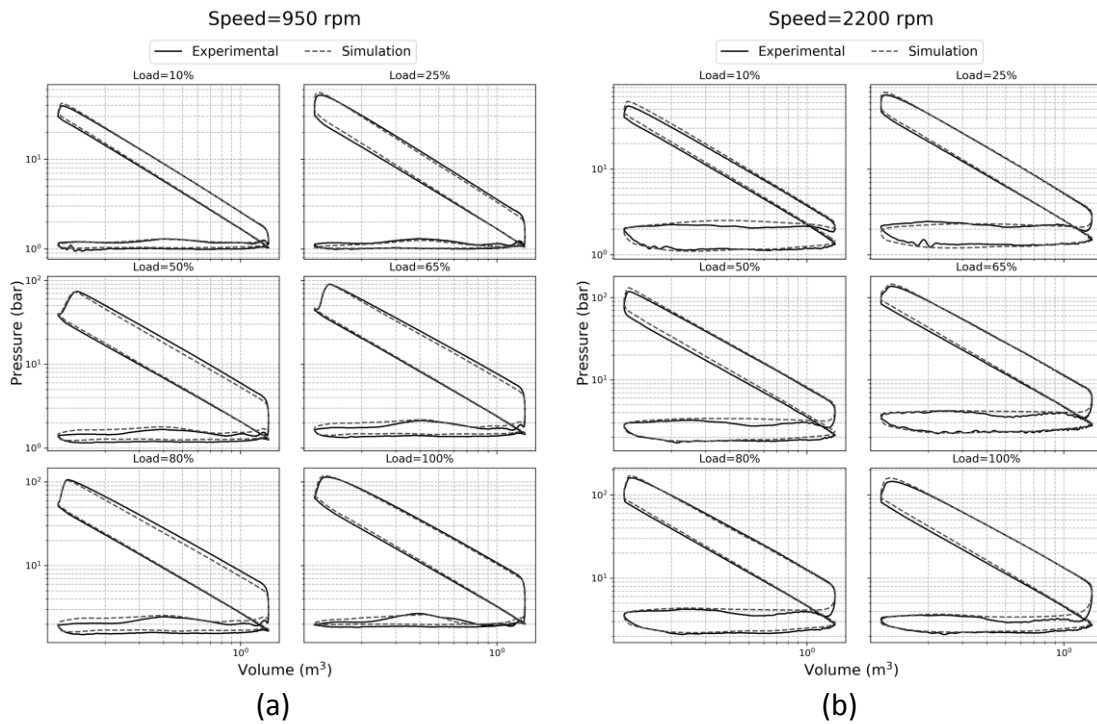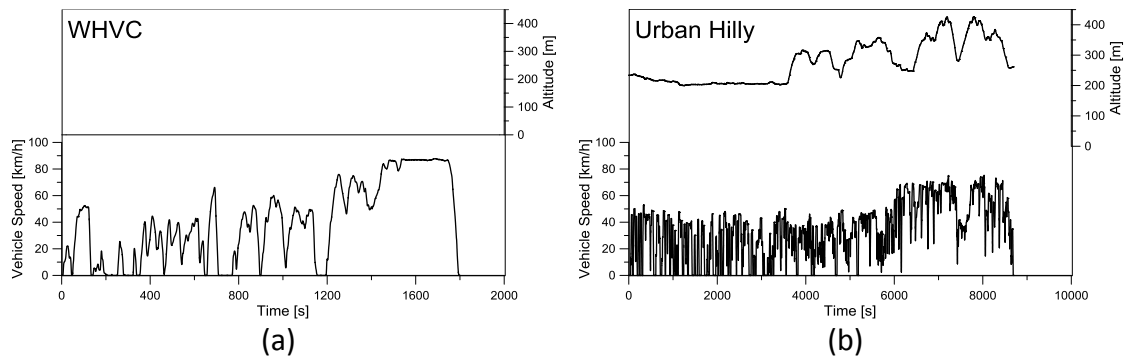

(a)

(b)

Figure A2- Pressure-Volume diagram with the experimental and simulation trace for 950 and 2200 rpm and engine load from 10% to 100% for DMDF ICE configuration.
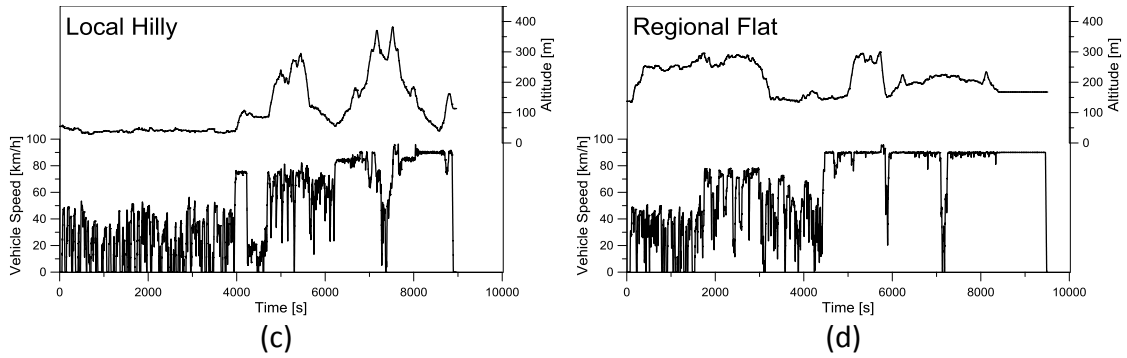
Appendix B

(a)

(b)

(c)   (d)

Figure B1 - Homologation (a) and real driving cycles (b)(c)(d) with vehicle speed and altitude against time.
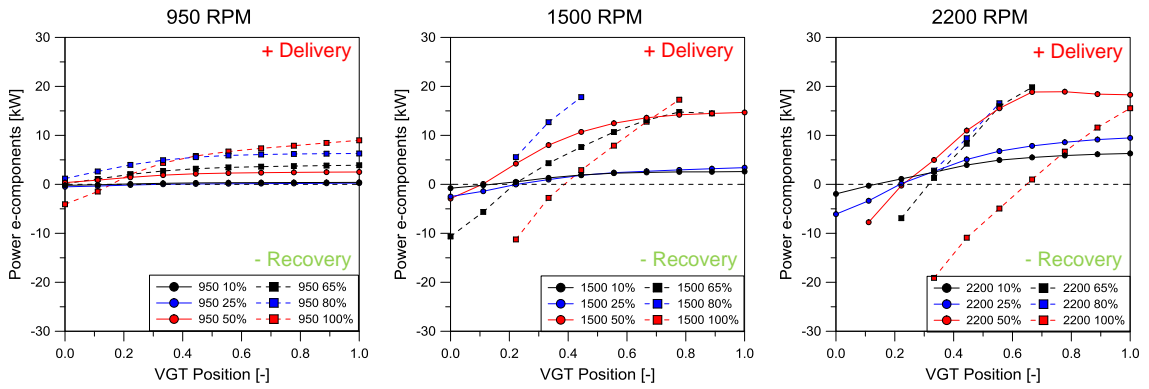
Appendix C

Figure C1- Power delivered by both e-components (eTC+e-EGR pump) at rotational engine speed of 950 rpm (a), 1500 rpm (b) and 2200 rpm (c) at different VGT rack positions.
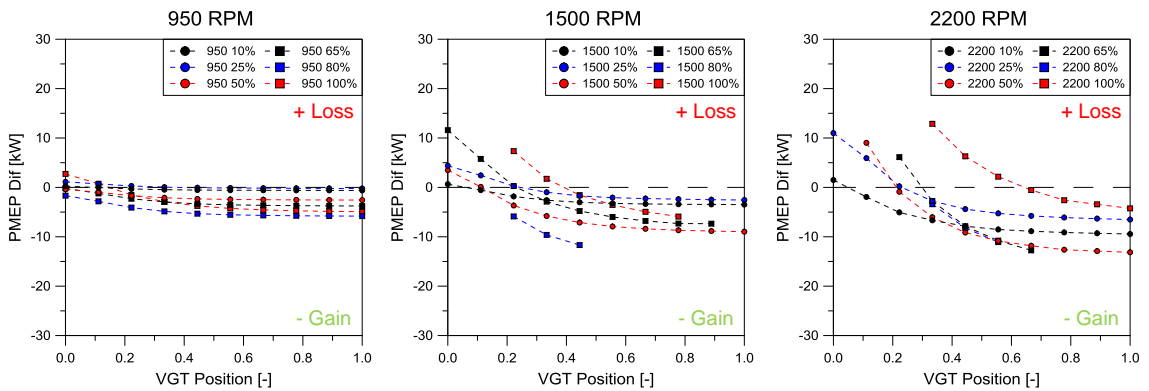

Figure C2 - Pumping mean effective pressure (PMEP) difference from DMDF LP&HP EGR calibration at rotational engine speed of 950 rpm (a), 1500 rpm (b) and 2200 rpm (c) at different VGT rack positions